

Reply to the interactive comment of Referee #2

The authors would like to thank the reviewer for the detailed commentary on the submitted manuscript. Below we provide replies to the suggestions that were made. It is our hope that these changes have improved the clarity of the presented results.

The authors agree that the final section of the paper is very lengthy. As the reviewer points out, the list of crucial assumptions provides a careful frame for the current study and we hope it will guide future studies of the Louisiana flooding event. In Section 7.2 we widen our view, and discuss further work regarding the flooding event and synoptic situation. We are of the opinion that it is important to mention these open questions, and to point out that probability attribution is not the only relevant study for this tragic event.

The authors disagree with the reviewer that the main focus of the paper is ‘an autopsy of the event in a climate context’. Indeed we report on the average return times of comparable precipitation events in the present climate, however the computation of these numbers are necessary steps towards calculating changes in statistics and providing the attribution to anthropogenic climate change.

As noted, including data from multiple models could strengthen the attribution statement. Unfortunately the models used for the attribution of the French and German precipitation extremes (HadGEM3-A N216 and EC-Earth 2.3 T159, Van Oldenborgh et al., 2016) were found to be unable to realistically simulate the full distribution of precipitation events on the Central U.S. Gulf Coast. Including data from these models would therefore not have strengthened the conclusions, as the only relevant statement that could be made is that these models do not capture the extremes and are therefore unsuitable for the analysis. The ensemble of regional model experiments from Weather@Home for the region of interest (Central America, CAM50, CAM25) is still in progress, for future analysis these experiments might indeed add valuable data when they become available.

Specific comments

p.2, l.35 – strange grammar, rephrase sentence

The sentence will be modified.

... The global climate models tell a similar story, in the most accurate analyses the regional probability of 3-day extreme precipitation increases by more than a factor 1.4 due to anthropogenic climate change. ...

p.2, l.52 – strange grammar, rephrase

The sentence will be modified.

... At that time the National Hurricane Center stated that the low pressure system might transform into a tropical depression if it moved to the Gulf of Mexico (Schleifstein, 2016). ...

p.3, l.72- explain “flood stage”

Flood stage is generally defined as the gage height at which overflow of the natural banks of a stream or river starts causing damage in the area. We will add this description to the manuscript.

... (USGS) registering above flood stage levels (levels at which overflow of natural banks starts to cause damage in the local area) at 30 sites and...

p.4, caption figure 2 – what is the pink area?

The shaded pink area indicates the 3-day period of maximum precipitation over the Central U.S. Gulf Coast (12-14 August). The figure caption will be modified to include this information.

... on the Amite River. Shaded pink areas indicate the 3-day period of maximum precipitation (12-14 August 2016). ...

p.4, ll.86-92 – while not irrelevant, the introduction is already very long, to actually have someone read this interesting paper it would be a good idea to shorten the introduction, this paragraph provides a good opportunity, but not the only one

The authors believe it is important to not the large societal impact of the event. This study was in part motivated by these significant human impacts of the Louisiana flooding event, as also noted in the introduction. We will shorten the paragraph slightly.

p.5, l.124 – add reference to what to examples or more explanation of what is meant by thermodynamic and dynamic responses and ‘weather type’. In particular the latter is quite ambiguous

Weather types refer to the previously described weather systems and events that may cause precipitation extremes. To avoid confusion and for consistency, we will replace the phrase ‘weather type’ with ‘weather system’.

We will add references to a review paper that describes different thermodynamic and dynamic responses. To avoid adding additional length to the introduction (see previous point) we won’t give an extensive list.

... may be different for different weather systems (O’Gorman 2015).

p.6, ll.143/144 – to avoid even more confusion than already exists in the community the term “event attribution” with or without added “extreme” or “probabilistic” would be better

We will change the term to ‘event attribution’.

... upon these methodologies for event attribution and also explores ...

p.7, ll.181-184 – what are the criteria to through out the other two considered models?

As in the French & German precipitation extremes study, we fitted the extreme tail of 3-day precipitation in the study area (a single representative grid point at the time) and compared the fit parameters of the GEV with those of the observations (copied straight from the lab book, not truncated to sensible precision):

(in 2016)	μ'	σ'	ξ	α
obs	51.792 (50.866... 52.786)	13.798 (13.137... 14.231)	0.118 (0.077... 0.136)	10.735 (7.701... 10.485)
HadGEM3-A	35.141 (34.199... 36.223)	12.982 (11.940... 13.576)	0.156 (0.107... 0.215)	1.539 (-1.779... 6.275)
EC-Earth 2.3	26.896 (26.603... 27.119)	5.165 (4.939... 5.340)	-0.034 (-0.072... -0.008)	1.502 (0.884... 2.135)

HadGEM3-A N219 has a 30% lower location parameter but almost the same scale parameter, hence much more variability in the high extremes when bias-corrected to the correct mean. EC-Earth T159 only has 50% of the location parameter, and not enough variability even after scaling with the location parameter and a wrong (negative) shape parameter. We concluded that neither model can represent the statistical properties of extreme precipitation in the study area.

The physical consideration is that the ~150 km resolution of EC-Earth T159 is not high enough to represent tropical storms well enough to capture their precipitation characteristics. The experience with FLOR vs HiFLOR in this area (Van der Wiel et al, 2016) suggests that the 60km resolution of HadGEM3-A N219 is also not sufficient.

p.7., l.198 & above – flux adjustment is not done in many models anymore for good reasons, very briefly discuss what the implications are for your study

We will add a comment on the implications.

... observed climatological state. This procedure reduces model biases of for example SSTs, tropical cyclones (Vecchi et al. 2014) and precipitation patterns. We assume the modeled response to changes in radiative forcing are not impacted by the flux-adjustment (see Section 7.1). The adjustment method is ...

p.9, l.241 – mention that in 7.1 you'll find the assumption not unjustified

We will add a comment.

and assume that the impact of the slow climate drift in each model experiment on the statistics of precipitation extremes is small (see justification in Section 7.1).

p.10, l.266 – add “a” between has & realistic

We will modify the sentence.

... 29-31 °N, 85-95 °W, which has a relatively homogenous average precipitation extreme magnitude ...

p.10, l.270 – do you mean the Golf region?

Yes indeed, we will add the specification.

For some analyses we then take the maximum over the Central U.S. Gulf Coast region.

p.11, l.295 – add reference for the moving block technique

We will add the reference.

Efron, B. and R.J. Tibshirani, R. J., 1998. An introduction to the bootstrap, Chapman and Hall, New York. 439pp.

p.13,l.339 – why do you use 3-day averages instead of sums?

For an attribution study to be completed within a rapid timeframe, analysis methods must be set up and ready to go before the event. In the current set up, the analysis tools (KNMI Climate Explorer) give average precipitation. Whether averages or sums are noted does not impact the conclusions, the average results may simply be multiplied by a factor 3 to get sums.

p.13, ll.352-355 – is there a reason for expressing the change in probability by a factor and the intensity in percentages? If not use the same measure for both.

The reason is that the changes in probability are usually much larger (one easily gets a factor four) than changes in intensity (tens of percents). Also, the two are often confused in popular accounts, keeping the units separate minimises the risk of this confusion.

p.14, l.361 – In which of the 2 sentences does figure 1 d,f belong?

There should be a reference to Figure 3d,f here, it will be corrected. It is then also clear that the reference is relevant for the sentence before.

... of 17% (C.I. 10%-21%), Figure 3d,f. The increase in probability ...

p.24, l.542 – up to 2100

We will modify the text.

does not change in the model world up to 2100, in spite of a different mix

p.25, ll.552-553 – this is a much better expression of your bias correction method than before

We will use this expression in the previous case (FLOR-FA, line 536 of the revised manuscript) and refer to that explanation in this place.

Because of model bias, we define our event to have the same return period as the gridded observations in 2016 (around 30 years, 115 mm/day).

We correct for this bias as we did for the FLOR-FA experiment (the 30 year event is 103 mm/day).

p.26, l.580 – is this a justified assumption?

Here, we assume forced changes over the period 1971-2015 dominates over internal changes, for example due to ENSO. ENSO is high-frequency and cancels out over this fairly long period: there have been many El Niño and La Niña events. Considering longer time scale modes of climate variability, the PDO also has trend very close to zero over this time period. The AMO has a strong trend, hence our investigation whether extreme rainfall in this area is connected to low-frequency Atlantic variability. The connection we found (with very low field significance, so it may have been spurious) would have lowered the probability of high precipitation, i.e., counter-acted the global warming signal.

p.28, table 3 – make clear in the table which experiment provides the proper attribution analysis

All model experiments mentioned in table 3 are used to create the attribution analysis. We will add a note making this explicit.

...Gulf Coast. Note the modeled changes can be attributed to anthropogenic climate change.

p.29, figure 15 – nice figure, but instead of using colours associated with models and in effect giving the same information twice it would be nice for the reader to have the proper attribution analysis highlighted instead

As described at the previous point, all model experiment data contribute to the attribution. The orange/red colours thus indicate the values that have been used for attribution. Values based on

observational data are on purpose coloured very differently (blue), to make the suggested distinction.

p.30, l.537 – management of what?

The sentence is indeed unclear. We will remove the statement on management and rather just mention societal impacts. The management implications (policy making etc.) may be considered to be part of societal impacts.

... Finally, we note some societal impacts of the findings.

p.30, section 7.1 – are the assumptions in any particular order? If so, what is it, if not it might be worth saying that.

The assumptions aren't in a particular order, though they are somewhat grouped by similarity. At the start of section 7.1 there is a list of topics for the crucial assumptions, we will modify the order to represent the order of the actual list.

... we have made the following crucial assumptions about the statistical distribution of precipitation extremes, the observations, the relationship between temperature and precipitation extremes and the models. We have tested ...

p.30, assumption 1) While you discuss later whether the grouping is justified or at least how it can be tested you do not comment on the GEV fit at all. Is that justified? Can we test that?

We write that the appropriateness of GEV fits should be tested (line 723 of the revised manuscript). A possible way to test this would be to analyze very long model integrations or very large ensembles, for which one can accurately compute the 1-in-500-year event and for which one can compute GEV statistics based on shorter blocks of modelled data.

p.32, assumption 9) – this is the strongest assumption I think and one that could be tested by using e.g. the weather@home model you've mentioned before, might be worth discussing why that has not been used (I assume no suitable runs were available but given that it is part of all other studies of rapid attribution publicised under World Weather Attribution for good reason it is worth mentioning)

The regional Weather@Home ensemble experiment for Central America (which includes the region of interest) is in progress and is not available at present.

p.32, l.720 – Finally? It is not your final point here. . . .

We will replace finally with furthermore.

... and Sutton 2009). Furthermore, the appropriateness of GEV fits in general.

p.33, ll.737-748 – this is a paragraph that could be easily written in a single sentence

The authors are of the opinion it is important to discuss the current scientific understanding on thermodynamic and dynamic changes separately and discuss how the former likely does not impact our results, while the latter might impact the presented changes. This is an active area of research that we wish to recognize in full.

p.33, l.751 – why did you not include the satellite data in the study? I'd assume it shouldn't take longer to analyse than the stations.

The period covered by satellite data (roughly 1979-present) is much shorter than the period covered by station observations (for this region 1891-present). The GEV estimates of return periods are better and more reliable if more data is included, therefore we have chosen to focus on two long datasets of observed station data. Secondly, satellite estimates of precipitation do not correspond well to ground-based observations, with biases that vary over time, making them ill-suited for trend analyses.

p.34,l.761 – for the kind of analysis you do high resolution seems only one factor, ensemble size is the other

High resolution is important for these model experiments, because tropical cyclones (and pseudo-tropical cyclones like the one that occurred in August 2016) need to be adequately simulated; the characteristics of tropical cyclones are more poorly simulated in models with resolutions of ~200km that are typical of the CMIP5 ensemble, but the two models used here have relatively realistic simulation of the statistics and characteristics (including rainfall distribution) of tropical cyclones (e.g., Vecchi et al. 2014; Murakami et al. 2015, 2016; Liu et al. 2016). Furthermore, in order to assess the statistics of the return times we require relatively long simulations (many 100s of years total), and we are unaware of any other high-resolution models that have been run for that length of time.

An ensemble of models with comparable capability to simulate the phenomena that lead to extreme rainfall in this region, and with experiments of sufficient length to assess the statistics, would allow one to further explore the structural uncertainty, but such an ensemble does not yet exist. We plan to repeat the analysis when these data have become available in HiResMIP.

section 7.2 – this section is rather disappointing in quality & added value given that it contains no insights in vulnerability and the latter part reads like an acknowledgement. I would recommend rewriting and drastically shortening to say why your study adds value instead of listing at length all the things you haven't done. It would be sufficient to mention that impact modelling and vulnerability assessment would be a great complementation.

In Section 7.1 we list and work through all assumptions and further work directly related to the present study. Section 7.2 is used to widen our vision, that was narrowed to only include extreme precipitation events after the introduction, and discuss avenues of further scientific investigation related to the flooding event. In our opinion, because of the rapid timeframe of the current study and its publication being one of the first on the Louisiana flood-inducing event, it is our task to explicitly mention that the current work is not the complete story.

The last three paragraphs (line 824 and onwards) provide insight into the procedure of rapid assessment. Though attribution analysis has become more routine since its introduction in 2005, the rapid attribution is relatively new. It is our hope that among the broader impacts of this study it serves the scientific community with a tool of how we believe such a study must be done. Therefore, we describe the modelling efforts that were already in place, without which the analysis could not have been done. And we describe a recent verification study of extreme precipitation in these models and in the region of interest, which was crucial in the decision to qualify these models for the study.

To address the confusion noted by the reviewer, we will alter the text.

Climate attribution studies such as this one can only be performed with pre-existing multi-centennial global simulations with high spatial resolution models. This allowed us to efficiently assess the impact of radiative forcing changes on regional extreme precipitation events. ...

p.35,II.3303 – end – it does not become clear how a synoptic analysis would provide anything useful in terms of decision making unless it is coupled with an assessment of the likelihood of the synoptic systems to occur hence this paragraph becomes a bit incomprehensible, again it would be better to highlight the strengths of your study and maybe refer to the Otto et al. paper if you want to highlight that the topic is not uncontroversial.

We describe how a synoptic attribution is fundamentally different from a probability attribution presented in the study. Each study is scientifically relevant, and each serves society in a different manner. Synoptic studies serve weather and emergency services, probability studies are more relevant for risk management in long-term policy. Otto et al. 2016 is presently provided as a reference to direct the reader to an exemplary paper on the topic for further reading.

References

Meehl, G.A., J.M. Arblaster, J.T. Sasullo, A. Hu, K.E. Trenberth (2011): Model-based evidence of deep-ocean heat uptake during surface-temperature hiatus periods, *Nature Climate Change*, 1, 360-364.

Van Oldenborgh, G.J., S. Philip, E. Aalbers, R. Vautard, F. Otto, K. Haustein, F. Habets, R. Singh, H. Cullen (2016): Rapid attribution of the May/June 2016 flood-inducing precipitation in France and Germany to climate change, *Hydrol. Earth Syst. Sci. Discuss.*, doi: 10.5194/hess-2016-308.

Rapid attribution of the August 2016 flood-inducing extreme precipitation in south Louisiana to climate change

Karin van der Wiel^{1,2}, Sarah B. Kapnick², Geert Jan van Oldenborgh³, Kirien Whan³, Sjoukje Philip³, Gabriel A. Vecchi², Roop K. Singh⁴, Julie Arrighi⁴, Heidi Cullen⁵

¹Program in Atmospheric and Oceanic Sciences, Princeton University, Princeton, U.S.

²Geophysical Fluid Dynamics Laboratory (GFDL), National Oceanic and Atmospheric Administration, Princeton, U.S.

³Royal Netherlands Meteorological Institute (KNMI), De Bilt, Netherlands

⁴Red Cross Red Crescent Climate Centre, The Hague, Netherlands

⁵Climate Central, Princeton, U.S.

Correspondence to: Karin van der Wiel (kwiel@princeton.edu) or Geert Jan van Oldenborgh (oldenborgh@knmi.nl).

Abstract.

A stationary low pressure system and elevated levels of precipitable water provided a nearly continuous source of precipitation over Louisiana, United States (U.S.) starting around 10 August, 2016. Precipitation was heaviest in the region broadly encompassing the city of Baton Rouge, with a ~~three~~3-day maximum found at a station in Livingston, LA (east of Baton Rouge) from 12–14 August, 2016 (648.3 mm, 25.5 inches). The intense precipitation was followed by inland flash flooding and river flooding and in subsequent days produced additional backwater flooding. On 16 August, Louisiana officials reported that 30,000 people had been rescued, nearly 10,600 people had slept in shelters on the night of 14 August, and at least 60,600 homes had been impacted to varying degrees. As of 17 August, the floods were reported to have killed at least thirteen people. As the disaster was unfolding, the Red Cross called the flooding the worst natural disaster in the U.S. since Super Storm Sandy made landfall in New Jersey on 24 October, 2012. Before the floodwaters had receded, the media began questioning whether this extreme event was caused by anthropogenic climate change. To provide the necessary analysis to understand the potential role of anthropogenic climate change, a rapid attribution analysis was launched in real-time using the best readily available observational data and high-resolution global climate model simulations.

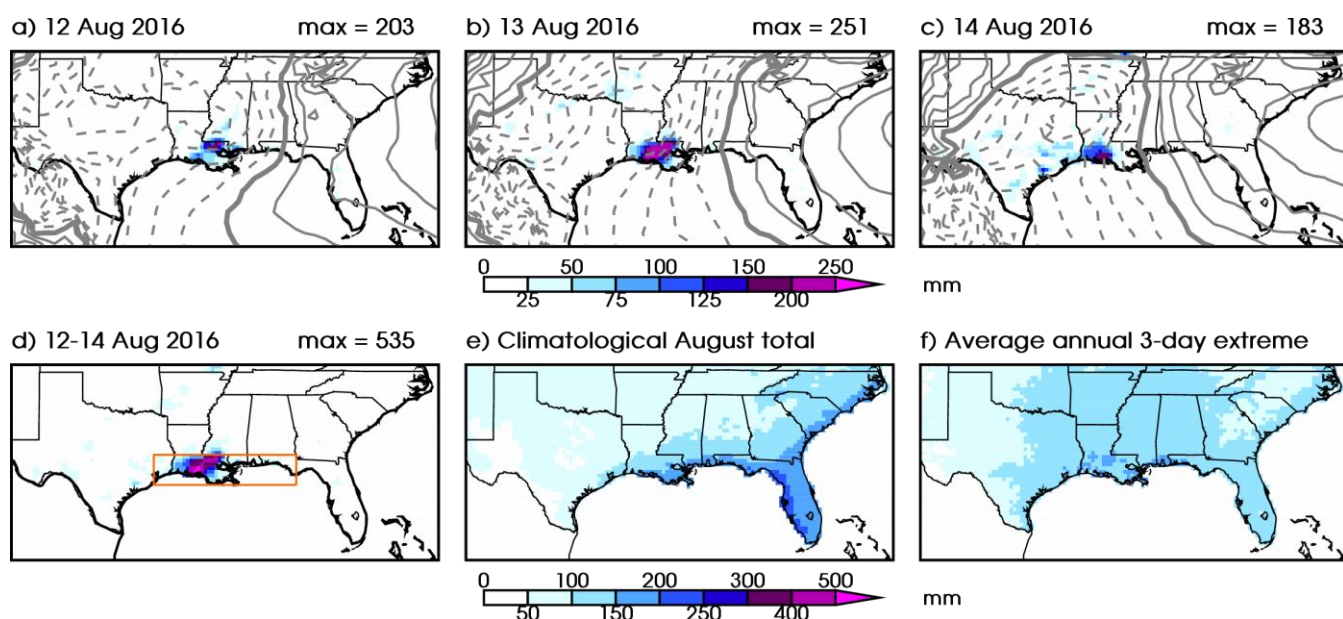
The objective of this study is to show the possibility of performing rapid attribution studies when both observational and model data, and analysis methods are readily available upon the start. It is the authors aspiration that the results be used to guide further studies of the devastating precipitation and flooding event. Here we present a first estimate of how anthropogenic climate change has affected the likelihood of a comparable extreme precipitation event in the Central U.S. Gulf Coast. While the flooding event of interest triggering this study occurred in south Louisiana, for the purposes of our analysis, we have defined an extreme precipitation event by taking the spatial maximum of annual 3-day inland maximum precipitation over the region: 29–31 °N, 85–95 °W, which we refer to as the Central U.S. Gulf Coast. Using observational data, we find that the observed local return time of the 12–14 August precipitation event in 2016 is about 550 years (95% confidence interval (C.I.): 450–1450). The probability for an event like this to happen anywhere in the region is

39 presently 1 in 30 years (C.I. 11-110). We estimate that these probabilities and the intensity of extreme
40 precipitation events of this return time have increased since 1900. A Central U.S. Gulf Coast extreme
41 precipitation event has effectively become more likely in 2016 than it was in 1900. The global climate models
42 tell a similar story, ~~in the most accurate analyses the regional probability of 3-day extreme precipitation~~
43 ~~increases by more than a factor 1.4 due to anthropogenic climate change, with the regional probability of 3-day~~
44 ~~extreme precipitation increasing due to anthropogenic climate change by more than a factor 1.4 in the most~~
45 ~~accurate analyses.~~ The magnitude of the shift in probabilities is greater in the 25 km (higher resolution) climate
46 model than in the 50 km model. The evidence for a relation to El Niño half a year earlier is equivocal, with
47 some analyses showing a positive connection and others none.

48 **1 Introduction**

49 In the second week of August, a storm system developed in the United States (U.S.) Gulf Coast region and
50 resulted in intense precipitation across south Louisiana in the region surrounding the city of Baton Rouge. The
51 highest concentration of precipitation fell over the 3-day period of 12-14 August (Figure 1a-d). Saturday, 13
52 August experienced the greatest total magnitude of precipitation and the broadest surface area of intense
53 precipitation during the storm. The National Oceanic and Atmospheric Administration (NOAA) Climate
54 Prediction Center (CPC) unified gauge-based gridded analysis of daily precipitation exhibits 25×25 km area
55 boxes with precipitation maxima reaching up to 534.7 mm (21.1 inches) over the 3-day period. In station
56 observations (a single point), a rain gauge in Livingston, LA (east of Baton Rouge) experienced an even higher
57 3-day precipitation total of 648.3 mm (25.5 inches). In places, the 3-day precipitation totals in Louisiana
58 exceeded three times that of the climatological August totals (historical average total precipitation that occurs
59 over 31-days, Figure 1e) and three times the average annual 3-day precipitation maximum (Figure 1f).

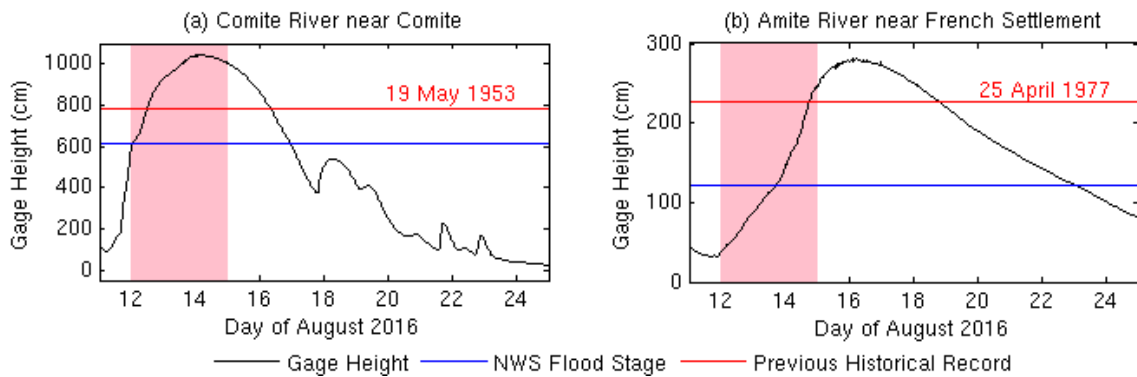
60 The intense precipitation formed due to a low pressure system that originated near Florida/Alabama on
61 5 August. At that time the National Hurricane Center stated that ~~the low pressure system~~ ~~it~~ might transform into
62 a tropical depression ~~after moving to the~~ ~~if it moved to the~~ Gulf of Mexico (Schleifstein 2016). Instead the
63 system remained over land and moved westward slowly. On 12 August it became near-stationary over Louisiana
64 (Figure 1a-c) allowing for the continuous development of thunderstorms in a localized area to the south and
65 southeast of the low pressure center. The stationary storm system and anomalously moist atmospheric
66 conditions (precipitable water exceeding 65 mm) created optimal conditions for high precipitation efficiencies
67 and intense precipitation rates. Though the system had a warm-core and some similarities to a tropical
68 depression, it never formed the closed surface wind circulation about a well-defined center that are needed to be
69 classified as one (National Weather Service 2016).



70

71 **Figure 1:** (a,b,c) Daily precipitation (shaded colors) and sea level pressure (grey contours, interval 1 hPa, 1015
 72 hPa contour thickened, lower contours dashed) for 12, 13 and 14 August, 2016. (d) 3-day precipitation sum 12-
 73 14 August, 2016. (e) August climatological total precipitation (1948-2015). (f) Average annual maximum 3-day
 74 precipitation event (1948-2015). Orange box in (d) shows the geographic region used for the analysis (29°-31°N,
 75 85°-95°W). Data from CPC unified gauge-based analysis of daily precipitation over the contiguous U.S. (2016
 76 data from the real time archive) and ECMWF operational analysis.

77 Historic freshwater flooding in the region encompassing Baton Rouge, Louisiana followed the extreme
 78 precipitation event. Provisional reports from 18 August, 2016 showed streamgauges managed by the United
 79 States Geological Survey (USGS) registering above flood stage levels levels at which overflow of natural banks
 80 starts to cause damage in the local area at 30 sites and found that out of 261 sites in all of Louisiana 50 were
 81 overtopped by floodwaters (Burton and Demas 2016). This was a complex event where provisional data from
 82 the USGS showed rivers responded responding to local precipitation as well as upstream and downstream
 83 conditions (Figure 2). For example, on the Comite River, a major drainage river for North Baton Rouge and its
 84 outlying districts, the provisional gauge height data exceeded the National Weather Service (NWS) flood stage
 85 from 12-16 August and even exceeded the previous height record (set 19 May, 1953). The Comite River hit its
 86 NWS flood stage level before the maximum precipitation fell in Central U.S. Gulf Coast ~~(Figure 1d)~~.
 87 Floodwaters were slow to recede due to flood stages downstream causing backwater flooding (upstream
 88 flooding caused by conditions downstream) in many neighborhoods (Burton and Demas 2016). Further
 89 downstream on the Amite River, provisional data showed that water levels exceeded the NWS floodstage from
 90 13-23 August and also exceeded the previous height record (set 25 April, 1977). Its levels declined more slowly
 91 and did not fall below floodstage until late on 23 August, due to drainage from the Comite and other tributaries
 92 upstream that hit peak floodstage days earlier (Burton and Demas 2016).



93

94 **Figure 2:** Hydrographs of gauge levels, NWS flood stage value and previous historical record for
 95 USGS station (a) 07378000 on the Comite River and (b) 07380200 on the Amite River. Shaded pink areas
 96 indicate the 3-day period of maximum precipitation (12-14 August 2016). Observed streamgauge information
 97 downloaded 25 August, 2016 from the USGS: <<http://waterdata.usgs.gov/la/nwis/uv?>>; provisional USGS data
 98 is subject to adjustment: <http://help.waterdata.usgs.gov/policies/provisional-data-statement>.

99 On 12 August the NWS issued flash flood warnings for parishes in south Louisiana, and activated the
 100 national Emergency Alert System which urged residents to move to higher ground. The Louisiana Coast Guard,
 101 National Guard, and civilian volunteers mobilized to rescue over 30,000 people from their flooded homes and
 102 cars (Broach 2016). By August 14, the federal government declared a major disaster, indicating that the severity
 103 of damage exceeded the local and state governments' combined capability to respond, initiating federal
 104 assistance for individuals and public infrastructure (Davies 2016, FEMA 2016, Stafford Disaster Relief and
 105 Emergency Assistance Act). The flooding impacted the state's agriculture industry with losses estimated in
 106 excess of \$110 million (Allen and Burgess 2016). Initial estimates also show that at least 60,600 homes were
 107 damaged, and thirteen people were killed due to the floods (Strum 2016). The American Red Cross, with FEMA
 108 and other federal and local agencies, provided shelter and emergency relief for 10,600 people initially displaced
 109 by the disaster, and the American Red Cross estimates that its ongoing relief efforts will cost \$30 million
 110 (American Red Cross 2016). To date, more than 110,000 people have registered for federal disaster assistance
 111 (FEMA, 2016). ~~FEMA has made grants totalling \$107 million available to disaster survivors for serious needs~~
 112 ~~including temporary rental assistance, and \$20 million in advance payments for National Flood Insurance~~
 113 ~~policyholders (FEMA 2016).~~

114 South Louisiana is a region where a number of phenomena can lead to flooding. For example, as a
 115 coastal region, it can experience saltwater flooding from a storm surge, when the low pressure and winds of a
 116 storm moving towards the coastline push coastal saltwater inland. This occurred in August 2005 when
 117 Hurricane Katrina impacted a broad swath of the Gulf Coast, including New Orleans, LA, with a large storm
 118 surge. Inland, precipitation can directly cause pluvial flooding by producing runoff in a region independent of a
 119 body of water (i.e. when more rain falls than can be soaked up by the ground) or fluvial flooding when water
 120 levels exceed the capacity of the river environment. For inland freshwater flooding, land surface conditions prior
 121 to an extreme precipitation event may increase the susceptibility of a region to both types of flooding, by
 122 saturating the soil (Tramblay et al. 2010, De Michele and Salvadori 2002) or increasing river levels (Pinter
 123 2006). Inland flood conditions can also be induced by water flowing through the river system after a storm due
 124 to capacity limitations, as evident along the Amite River in August 2016 (Figure 2b) due to upstream flood
 125 conditions making their way downstream. Flooding can be influenced by remote meteorological conditions as

126 river networks connect regions over vast areas. Louisiana had most recently experienced widespread inland
127 flooding in March-April 2016. Although inland freshwater flooding occurs due to a combination of the level of
128 extreme precipitation and its interaction with the land surface and river system, including human modifications
129 to those systems and responses to events, we have chosen to focus our rapid attribution study on one portion of
130 the problem: understanding the present and potentially climate change-influenced probability of extreme
131 precipitation events like the one which occurred in August 2016.

132 Synoptic forcing for precipitation extremes in the Gulf Coast region includes both mid-latitude weather
133 (cold core systems fueled by baroclinic instability), and tropical weather (warm core systems with barotropic
134 instability). Extreme precipitation has historically been classified into 3 types of events: frontal systems, tropical
135 systems, and air mass systems. Each of these categories can be further broken down; e.g. tropical systems
136 ranging from easterly waves to hurricanes, frontal systems including interactions between the polar jet and moist
137 air masses from the Gulf, squall lines, or mesoscale convective systems, and air mass systems that may include
138 heavy rainfall from upper air disturbances, or convective storms that form because of daytime heating (Keim
139 and Faiers 1996). The variety of weather systems that can give rise to precipitation extremes in the region
140 complicates the statistical analysis of the extremes and requires climate models to capture the entire distribution
141 in a realistic manner. Also, the response to radiative forcing may be non-linear: thermodynamic and/or dynamic
142 changes may be different for ~~different each~~-weather systems (O’Gorman 2015)type.

143 In this article, we analyze the historical context and changes in statistics of extreme precipitation like
144 the one experienced during August 2016 in south Louisiana by defining an extreme event by its local or regional
145 maximum 3-day precipitation. We have focused our analysis on stations or land surface grid cells in the region:
146 29–31 °N, 85–95 °W (illustrated by the ~~red-orange~~ box in Figure 1d), which we hereafter refer to as the “Central
147 U.S. Gulf Coast”. Here we report the results of our rapid attribution study conducted by several organizations
148 within two weeks of the event. The need for a rapid attribution study arises from the current intense public
149 discussion that results from the significant societal impacts of this particular event and a continuous general
150 interest in climate change. Media coverage following the event has linked into the growing body of scientific
151 evidence that precipitation extremes are expected to increase due to the greater moisture content of a warmer
152 atmosphere following Clausius-Clapeyron scaling (O’Gorman 2015, Lenderink and Attema 2015, Scherrer et al,
153 2016): e.g. “Disasters like Louisiana floods will worsen as planet warms, scientists warn” (Milman 2016),
154 “Flooding in the South looks a lot like climate change” (Bromwich 2016). However, specific scientific
155 statements for the event as observed in south Louisiana cannot be made based on general assessments of the
156 connection of global warming and extreme rainfall. While attribution studies at a more traditional scientific pace
157 (several months up to a year later) are important and add to scientific understanding of changing extremes,
158 reporting results recently after an extreme event may enhance the societal understanding of climate change and
159 extreme weather, and provide often requested information for management decisions following the event.

160 The methodologies employed in this study are used regularly in the literature and were previously
161 applied to the rapid attribution of the French and German 2016 flooding event (Van Oldenborgh et al. 2016) and
162 of Storm Desmond over the UK in 2015 (Van Oldenborgh et al. 2015). The presented analysis builds upon these
163 methodologies for ~~event anthropogenic climate change~~-attribution and also explores the role of climate
164 variability. The trends and internal climate variability of extreme precipitation is investigated in station
165 observations, gridded gauge-based precipitation analysis, and high-resolution global climate model simulations.

166 Since this paper aims to provide a first attribution assessment of the 2016 south Louisiana extreme event, we
167 have provided a detailed data and methods section (Section 2) in which our data sets, statistical calculations for
168 return periods and trends and data set validation methodologies are described. The rest of the paper is organized
169 as follows: Section 3 provides observational analysis. In Section 4 we evaluate the suitability of the global
170 climate models. Model analysis is provided in Section 5. Section 6 synthesizes our conclusions. In Section 7 we
171 provide a detailed discussion of crucial assumptions and their potential impact on the results, further avenues of
172 research and implications of this work.

173 **2 Data and methods**

174 **2.1 Observational data**

175 We utilize both point station observations and gridded analysis in this paper. The point station data are from the
176 Global Historical Climatology Network daily product (GHCN-D) version 3.22 (Menne et al. 2012, 2016). The
177 data set provides daily observations for stations worldwide. Data is quality controlled before becoming available
178 in near-real time. Inside the defined Central U.S. Gulf Coast (Figure 1d), 324 stations with a minimum of 10
179 years of data are available for the period 1891 to present (August 2016). However, not all stations provide data
180 for the entire period, and spatial proximity between stations means that not all data points provide independent
181 information ([see Section 7.1](#)). Therefore for some analyses a smaller selection of the available stations is taken
182 into account. Selection criteria are described in the relevant sections.

183 The gridded analysis used here is the product of the NOAA ~~Climate Prediction Center (CPC)~~CPC
184 Unified Gauge-Based Analysis of Daily Precipitation over the contiguous U.S. (Higgins et al. 2000). The data
185 set interpolates point station data on a $0.25^{\circ} \times 0.25^{\circ}$ uniform latitude-longitude grid, based on the optimal
186 interpolation scheme of Gandin and Hardin (1965). The CPC dataset covers the period 1 January 1948 to
187 present (August 2016), data from 2007 onwards has been made available in real time. Because this is a gridded
188 product, daily precipitation sums represent an areal average ($0.25^{\circ} \times 0.25^{\circ}$) rather than a point measurement.
189 Therefore precipitation extremes are expected to be of smaller magnitude in the gridded product (Chen and
190 Knutson 2008), as was noted for the south Louisiana event above (3-day total maxima of 534.7 mm in the CPC
191 gridded versus 648.3 mm in the point station data). The gridded analysis and the individual station data are not
192 independent, as the precipitation station data is the underlying source for the gridded analysis; consequently,
193 changes in gauge station density in space and time (as discussed above for GHCN-D) also impact the gridded
194 analysis. We note that, for comparisons with climate models - in which precipitation represents area averages,
195 and not point values - the area-averaged precipitation values from the gridded analysis are likely more
196 meaningful for comparison with models than point station data (Chen and Knutson 2008, Eggert et al, 2015).

197 We use the National Aeronautics and Space Administration (NASA) Goddard Institute for Space
198 Science (GISS) surface temperature analysis (GISTEMP, Hansen et al. 2010) for estimates of the development
199 of global mean surface temperature over time. This gridded data set is based on the GHCN point station data
200 over land, NOAA Extended Reconstructed Sea Surface Temperature (ERSST, Huang et al. 2015) version 4 over
201 oceans and Scientific Committee on Antarctic Research (SCAR) point station data for Antarctica.

202 2.2 Model and experiment descriptions

203 Many of the meteorological phenomena that cause extreme precipitation at the [Central](#) U.S. Gulf Coast are
204 small-scale, therefore only high-resolution models can simulate them realistically. We verified that the Royal
205 Netherlands Meteorological Institute (KNMI) EC-Earth 2.3 T159 experiments (~150km, Hazeleger et al. 2012)
206 and the United Kingdom (U.K.) Met Office HadGEM3-A N216 (~60km, Christidis et al. 2013) models do not
207 realistically represent precipitation extremes in the region.

208 We therefore use two higher-resolution global climate models in our analysis from the NOAA
209 Geophysical Fluid Dynamics Laboratory (GFDL). Both models were developed from the GFDL Coupled Model
210 version 2.1 (CM2.1, Delworth et al. 2006) using a cubed-sphere finite volume dynamical core (Putman and Lin
211 2007) with 32 vertical levels. Atmospheric physics are taken from the GFDL Coupled Model version 2.5
212 (CM2.5, Delworth et al. 2006, 2012). The two models share the same ocean and sea ice components with a 1°
213 horizontal resolution, but differ in their atmosphere and land horizontal resolution. In the Forecast-oriented Low
214 Ocean Resolution model (FLOR, Vecchi et al. 2014), there are 180 points along each cubed-sphere finite
215 volume dynamical core face (FV3-C180), which relates to a resolution of 0.5° per cell along the Equator. This
216 has been interpolated to a 0.5°×0.5° uniform latitude-longitude grid. In the high-resolution version of the model
217 (HiFLOR, Murakami et al. 2016), there are 384 points along each face (FV3-C384) on the cubed-sphere finite
218 volume dynamic core, which relates to a resolution of 0.23° per cell along the Equator. This has been
219 interpolated to a 0.25°×0.25° uniform latitude-longitude grid. For FLOR we use a flux-adjusted version of the
220 model (FLOR-FA), in which atmosphere-to-ocean fluxes of momentum, enthalpy and freshwater are adjusted to
221 bring the simulated fields closer to their observed climatological state. [This procedure reduces model biases of](#)
222 [for example SSTs, tropical cyclones \(Vecchi et al. 2014\) and precipitation patterns. We assume the modeled](#)
223 [response to changes in radiative forcing are not impacted by the flux-adjustment \(see Section 7.1\).](#) The
224 adjustment method is described in detail in Vecchi et al. (2014). Descriptions on how to access the data used in
225 this study are provided in the Data Availability section.

226 Table 1 describes six different global coupled model experiments that have been performed using
227 FLOR-FA and HiFLOR, which —for each model— differ in the type of radiative forcing that is prescribed, thus
228 allowing us to assess the impact of radiative forcing on the statistics of weather extremes in these models. With
229 FLOR-FA there are two sets of experiments. First, we made use of a multi-centennial integration in which
230 values of radiative forcing agents (solar forcing, anthropogenic and natural aerosols, well-mixed greenhouse
231 gases, ozone, etc.) are prescribed to remain at levels representative of a particular time - the mid-19th century in
232 this case (Jia et al. 2016); radiative forcing agents are prescribed at the 1860 values following the protocol of the
233 Fifth Coupled Model Intercomparison Project (CMIP5, Taylor et al. 2009). These types of experiments with
234 global climate models are often referred to as “control” experiments (“pre-industrial control” in this particular
235 case) but here we label this class of experiments as “static radiative forcing” experiments, since with HiFLOR
236 we fix radiative forcing at a number of levels. In the static radiative forcing experiments the years of the
237 integration bear no relation to the real world calendar. The second set of experiments with FLOR-FA is a suite
238 of five realizations (or “ensemble members”) in which the radiative forcing is prescribed to follow estimates of
239 past and future radiative forcing changes over the period 1861-2100 (Jia et al. 2016); the forcing agents for the
240 period 1861-2005 are prescribed to follow the CMIP5 historical experiment protocol, and for the period 2005-

241 2100 they follow the CMIP5 Representative Concentration Pathway 4.5 (RCP4.5), which represents the medium
 242 range greenhouse gas emissions scenario (Van Vuuren et al. 2011). The five realizations of 1861-2100
 243 experiments differ only in their initial conditions on January 1, 1861, which are taken from five different years
 244 from the long FLOR-FA preindustrial static forcing experiment. In these experiments, the calendar of the
 245 experiments is connected to the history of radiative forcing - but the internal climate variations (e.g., El Niño
 246 events) and weather fluctuations (e.g., individual storms) are not constrained to follow their observed sequence.
 247 The static climate experiment has a slow drift because the slow climate components, notably the deep ocean,
 248 were not in equilibrium at the beginning of the run, this is most noticeable in the first 1000 years of the
 249 integration.

250

251 **Table 1:** Global coupled model experiments performed with the FLOR-FA and HiFLOR models.

Model	Type of forcing	Representative year of forcings	No. of ensembles	No. of modeled years in total
FLOR-FA	Static radiative forcing	1860	1	3550
FLOR-FA	Time-varying radiative forcing	1861-2100	5	1200 (5 realizations of 240 years)
HiFLOR	Static radiative forcing	1860	1	200
HiFLOR	Static radiative forcing	1940	1	75
HiFLOR	Static radiative forcing	1990	1	300
HiFLOR	Static radiative forcing	2015	1	70

252

253 With HiFLOR, there are four experiments to explore the climate sensitivity of the statistics of weather
 254 events through static radiative forcing experiments at levels representative of particular times: preindustrial
 255 conditions (fixed at 1860 values), mid-20th Century (fixed at 1940 values), late-20th Century (fixed at 1990
 256 values), and early 21st Century (fixed at 2015 values). The value of radiative forcing agents in these experiments
 257 is prescribed from either the CMIP5 Historical Forcing protocol (for the 1860, 1940 and 1990 static forcing
 258 experiments) or from the CMIP5 RCP4.5 protocol (for the 2015 static forcing experiment); and the coupled
 259 atmosphere-land-ocean-sea ice state of the model is left to evolve freely. These simulations have been integrated
 260 for different lengths of time (Table 1, last column), over which they generate their own climate under the fixed
 261 forcing; longer integrations allow us to better estimate the statistics of climate extremes, but these were the
 262 lengths of integrations available as of 15 August, 2016.

263 There are many fewer model years available with HiFLOR than FLOR-FA because the HiFLOR model
 264 was developed more recently, and because the HiFLOR model is substantially more computationally intensive
 265 (~6× the computer resources required for one year of integration) than FLOR-FA. The four HiFLOR static
 266 forcing experiments are initialized from the same ocean, atmosphere, land and sea ice initial conditions, which
 267 are representative of the observed state in the late 20th century, and the four experiments are not in radiative
 268 balance through the length of integration (the 1860 experiment has a negative top of atmosphere balance, while
 269 the 1940, 1990 and 2015 experiments have positive balances). Therefore these static climate experiments each
 270 exhibit an initial rapid (~20 year) adjustment away from the late-20th century observed initial conditions, and a
 271 slower climate drift reflecting the top of atmosphere imbalance over the length of the integration. We exclude
 272 the first twenty years of each integration from our analysis, and assume (see Section 7.1) that the impact of the
 273 slow climate drift in each model experiment on the statistics of precipitation extremes is small (see justification
 274 in Section 7.1).

275 In addition to the coupled model experiments discussed above, in which the history of sea surface
 276 temperatures (SSTs) in the models emerges from the dynamics of the models and the changes in radiative
 277 forcing, for HiFLOR a set of variable forcing experiments were run over 1971-2015 in which the model is
 278 constrained by both historical radiative forcing and the observed history of monthly SST (Table 2). These
 279 experiments can be used to connect the statistics of rainfall extremes to the detailed history of SSTs that
 280 occurred over the past 45 years, part of which was a response to radiative forcing changes and part of which
 281 emerged from internal climate variations. Furthermore by construction, these experiments have a substantially
 282 smaller SST bias than the free running versions of HiFLOR, as the statistics of weather extremes and their
 283 connection to larger-scale climate can be substantially affected by SST biases (e.g. Vecchi et al. 2014;
 284 Krishnamurthy et al. 2015; Pascale et al. 2016). These experiments are described in more detail in Murakami et
 285 al. (2015) and Van der Wiel et al. (2016). The model SST was restored to the interannually varying observed
 286 field (SST_T) Met Office Hadley Centre SST product (HadISST1.1, Rayner et al. 2003) by adding an extra term
 287 to to the modeled SST tendency:

$$288 \quad \frac{dSST}{dt} = 0 + \frac{1}{\tau}(SST_T - SST) \quad \text{Eq. (1)}$$

289 with τ the restoring time scale (three ensemble members were produced with $\tau = 5$ days, three with $\tau =$
 290 10days).

291

292 **Table 2:** Restored SST experiments performed with the HiFLOR model.

Model	Type of forcing	Representative year of forcings	No. of ensembles	No. of modeled years in total
HiFLOR	Time-varying radiative forcing (CMIP5 Historical and RCP4.5); SSTs restored to observed monthly observations	1971-2015	6	270 (6 realizations of 45 years)

293 2.3 Defining an extreme event and its statistics

294 To classify the August 2016 south Louisiana flooding event, we must choose a definition for the event to guide
 295 our statistical analysis of observations and model experiments. We have chosen to classify extremes using
 296 multi-day averaged precipitation rather than single-day precipitation, to reflect the aspects of the event that
 297 resulted in the flooding of several rivers in the area. The following steps are taken to calculate our event
 298 statistics in the model and observations.

299

- 300 1. We create 3-day precipitation averages in station points/grid cells over land found in the Central U.S.
 301 Gulf Coast: 29–31 °N, 85–95 °W, which has a relatively homogenous average precipitation extreme
 302 magnitude (Figure 1f). This provides us with, for each point in space, 365 values per year (366 in leap
 303 years) for each station point/grid cell, except the last and first years in the record when there are 364
 304 values per year (365 in leap years), since the first January 1 and last December 31 are dropped.
- 305 2. We then, at each point in space, calculate the annual maximum for each year and define it as the local
 306 extremum for the year to create a set of extreme values for further analysis.
- 307 3. For some analyses we then take the maximum over the Central U.S. Gulf Coast region. We have
 308 carefully documented in the main text when this is the case.

309 4. In the static forcing model experiments, we disregard the first 20 years of data to allow for some initial
 310 spin-up of the model in each new static forcing state.

311

312 In order to estimate the observed return periods using the 3-day annual events found above, we fit the
 313 resulting data to a Generalised Extreme Value (GEV) Distribution (Coles 2001) in a similar manner as
 314 previously done for rapid attribution of the 2015 storm Desmond over the UK (Van Oldenborgh et al. 2015) and
 315 for the rapid attribution of the 2016 flooding in France and Germany (Van Oldenborgh et al. 2016). We first
 316 analyze the GEV distribution of observations and model simulations to determine if they represent the statistics
 317 of ~~summertime~~ extreme precipitation events sufficiently to employ them in further work. To account for
 318 possible changes due to anthropogenic climate change over time, we scale the distribution with the 4-year
 319 smoothed global mean temperature (GISTEMP for observational analysis, modeled global mean 2m air
 320 temperature for model analysis), a measure of the uniform global climate response to forcing. The GEV function
 321 is represented by:

$$\begin{aligned}
 322 \quad F(x) &= \exp \left[- \left(1 + \xi \frac{x-\mu}{\sigma} \right)^{1/\xi} \right], & \text{Eq. (2)} \\
 323 \quad \mu &= \mu_0 \exp \left(\frac{\alpha T'}{\mu_0} \right), \\
 324 \quad \sigma &= \sigma_0 \exp \left(\frac{\alpha T'}{\mu_0} \right).
 \end{aligned}$$

325 Where μ is the location parameter, σ is the scale parameter, and ξ represents the shape parameter of the curve.
 326 The ratio of σ/μ reduces to the constant σ_0/μ_0 . The fit is estimated using a maximum likelihood method where
 327 σ, μ_0, σ_0 and ξ are varied. There is a penalty term on ξ : a Gaussian with a width of 0.2 is added to the likelihood
 328 function such that values larger than ~ 0.4 are penalized as unphysical. This is mainly used to restrain fits to the
 329 1000-member non-parametric bootstrap that is used to estimate uncertainty. All years are assumed to be
 330 independent for this analysis, however correlations between proximate stations or ensemble members (when
 331 available) are taken into account with a moving block [bootstrap](#) technique ([Efron and Tibshirani 1998](#)). The
 332 average number of dependent stations will be noted in the analysis.

333 The GEV is first estimated for observational data to provide a baseline for validation. We then evaluate
 334 the individual models by assessing the extent to which the GEV fit parameters (μ, σ and ξ) are similar to those
 335 fitted to the longest available observational analysis (GHCN-D). As in Van Oldenborgh et al. (2016),
 336 multiplicative bias correction is employed for the model data, which tends to improve the similarity of the GEV
 337 fit from the model and the observations.

338 After a conditional GEV fit has been computed, with global mean surface temperature as the covariate,
 339 Eq. (2) can be inverted to find the probability of the south Louisiana event in any year. We thus estimate the
 340 probability for the south Louisiana event in 2016, p_1 , and its probability in some earlier year, p_0 - taken as [1860](#),
 341 [1900](#) or the first year with available data if that is later. ~~This~~ year ~~1900~~ is taken as representative for a climate
 342 that has not yet been strongly influenced much by anthropogenic climate change. The probabilities for an event
 343 with a magnitude at least as great as that observed in south Louisiana in each year, i , can be expressed as return
 344 times, τ_i , by:

$$345 \quad \tau_i = 1/p_i \quad \text{Eq. (3)}$$

346 The ratio of probabilities or return periods from different years is known as the risk ratio where:

$$347 \quad RR = p_1/p_0 = \tau_0/\tau_1 \quad \text{Eq. (4)}$$

348 The risk ratio is a measure of how the likelihood of an event has changed in the target year (*e.g.*, 2016) versus a
349 reference year (*e.g.*, 1900). A *RR* value of 1 would mean that the likelihood has not changed in the baseline year
350 versus the target year. This ratio is therefore an indicator of changes in likelihood, but alone it cannot attribute
351 this difference to a given mechanism.

352 There are multiple methods available to evaluate the impact of radiatively-forced climate change on the
353 change in likelihood of events. For FLOR-FA, we repeat the analysis for the observations using data from the
354 transient experiments. The natural variability from an ensemble member of the model is uncorrelated with that
355 of other ensemble members, or the real world, so common changes in the ensemble members are therefore due
356 to the prescribed external forcings. Multi-decadal changes over the past century are dominated by anthropogenic
357 forcings. For the highest-resolution global climate model, HiFLOR, we fit a concatenated time series of
358 maximum precipitation and the corresponding global mean temperatures from the four static forcing
359 experiments to Eq. (2). Furthermore, in HiFLOR we fit the trends in extremes in the variable forcing 6-member
360 ensemble covering 1971-2015. These simulations feature restored SSTs which reduce oceanic temperature
361 biases compared to a fully free running ocean component and include the same oceanic variability as the real
362 world (*e.g.* El Niño events, North Atlantic decadal variability).

363 We use the same procedure to investigate the effect of ENSO on extreme precipitation on the U.S.
364 Central Gulf Coast, replacing the smoothed global mean temperature by an index of the strength of El Niño as
365 covariate in Eq. (2). As the 2016 flooding occurred half a year after a strong El Niño event, we take as an index
366 a detrended version of the Niño3.4 index with a lag of six months. The detrending is done by subtracting the
367 average SST over 30 °S–30 °N.

368 **3 Observational analysis**

369 We here describe the character of the statistical distribution of observed precipitation extremes and their trends
370 in the GHCN-D point station data and the CPC gridded analysis by fitting to a time-dependent GEV distribution
371 (described in Section 2.3). Due to the many different meteorological phenomena that can lead to precipitation
372 extremes in the Central U.S. Gulf Coast, we assess the extent to which the GEV gives a satisfactory description
373 of the underlying data. We frame the results around measures of the probability per year of an event at least as
374 intense as the 2016 south Louisiana event (expressed as a return time), and the change of return time from the
375 beginning of the dataset to present (risk ratio). These return times can be assessed at a local scale (the expected
376 wait time for an event *at a particular place*) or at a regional scale (the expected return time for an event
377 *somewhere* in the Central U.S. Gulf Coast). Because the spatial scale of the most extreme precipitation events is
378 substantially smaller than the whole region, the local return times are longer than the regional return times. This
379 observational analysis on its own is only able to detect whether a trend is present, but cannot ascribe cause(s) to
380 these trends. Note that from here onwards we will principally report 3-day average precipitation values rather
381 than 3-day precipitation sums, unless stated otherwise.

382 **3.1 Point station data**

383 We first analyze point station data, as extremes are affected by interpolation and station density, using the
384 GHCN-D v3.22 dataset. This first analysis does not take the spatial maximum (Step 3 in Section 2.3), but

385 analyzes all stations in the region with at least 10 years of data. This gives 324 stations with 12536 station years
386 with data (Figure 3a), though it is crucial to note that they are not all statistically independent. The highest
387 observed value at these gauges in 2016 is 216.1 mm/day at Livingston, LA on 12–14 August (648.3 mm, three-
388 day sum).

389 Fitting these data to a time-dependent GEV distribution as described in Section 2.3 gives a reasonable
390 description of the data (Figure 3c,e), although the fit is shaped mainly by the lower-intensity events and the
391 highest-intensity events align closer to the lower bound. It should be noted that for each point station in the
392 dataset, on average another 18 are correlated with $r > 1/e$, so the number of degrees of freedom is much less
393 than the number of points. Overall it is surprising that all different meteorological situations that can give rise to
394 extreme precipitation (as laid out in Section 1) can be described with a single GEV function.

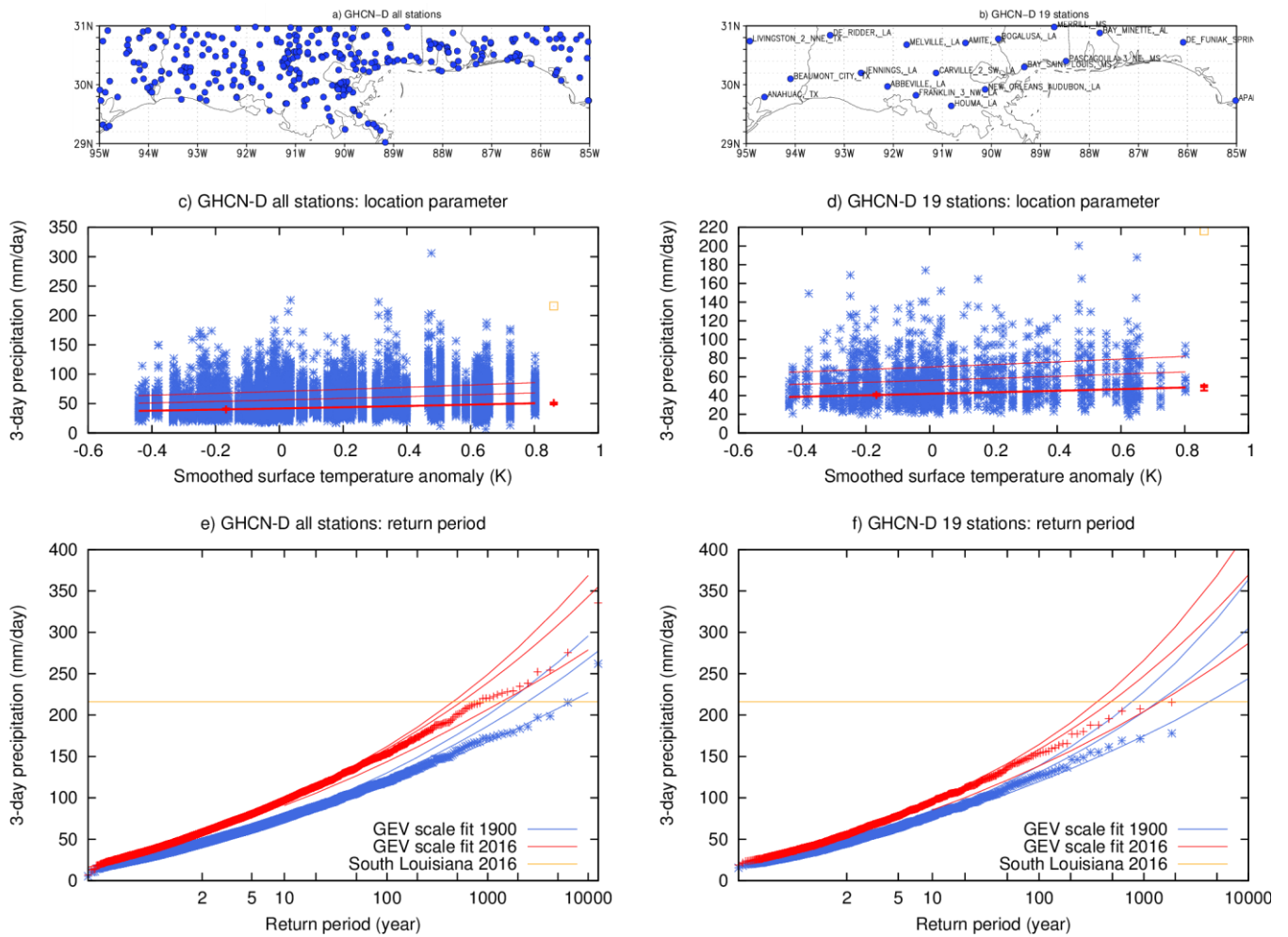
395 The local return time of a 216.1 mm/day event at a station in 2016 is about 550 yr (95% Confidence
396 Interval, C.I., 450-1450 yr). The probability of a 3-day precipitation event at a station with 216.1 mm/day or
397 more has increased by a factor 4.5 (C.I. 3.0-5.5) since 1900 in this analysis. This corresponds to an increase in
398 intensity for a given return time of 22% (C.I. 16%-22%).

399 This fit of all data available may be influenced by the spatially and temporally varying numbers and
400 locations of stations. We therefore evaluate the impact of these changes in sampling on the results by limiting
401 the analysis to stations with at least 80 years of data and at least 0.5° of spatial separation between stations. This
402 leaves 19 stations with 1849 station years (Figure 3b), which results in 2.3 stations per degree of freedom on
403 average. This analysis gives similar results: a return time of about 500 years (C.I. 360-1400) and an increase in
404 probability of a factor 2.8 (C.I. 1.7-3.8), corresponding to an increase in intensity of 17% (C.I. 10%-21%),
405 Figure 4d3d,f. The increase in probability is less than in the full station sample, although compatible within the
406 2σ uncertainties. ~~As the impact of inhomogeneities is smaller when considering longer time series, we use this
407 result from the 19 GHCN-D point stations for the trend estimate.~~

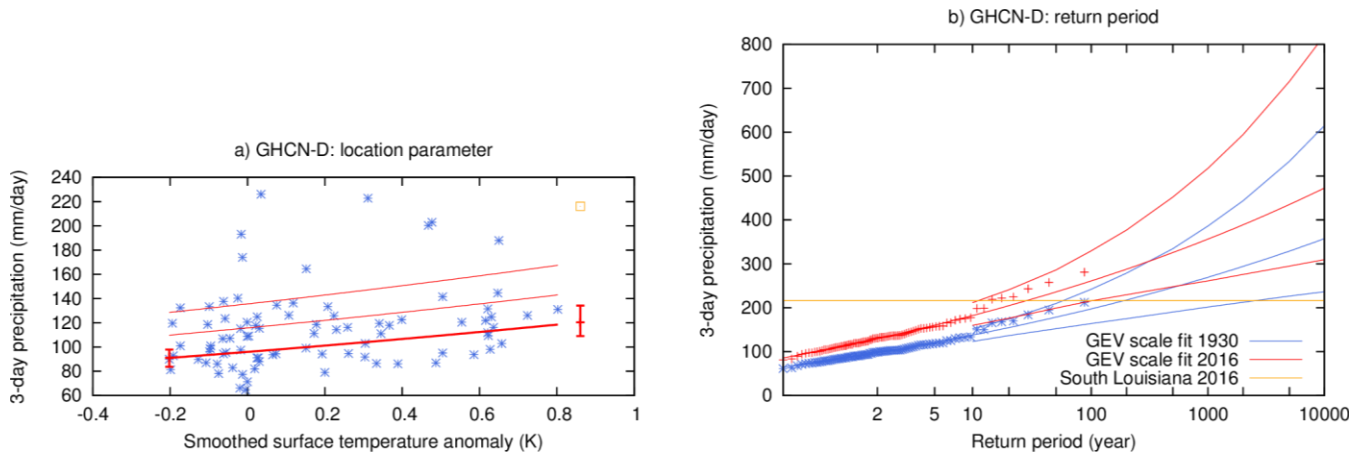
408 Our final analysis of point station data focuses on the most intense events only by considering the
409 spatial maximum of 3-day averaged precipitation anywhere in the Central U.S. Gulf Coast (Step 3 in Section
410 2.3). This answers the question how likely an event, like that of south Louisiana 2016 or worse, was anywhere
411 in the region, rather than at a specific place. In the point station data, the spatial maximum is only homogeneous
412 when the number of stations does not vary by much. We therefore again consider only those stations with at
413 least 80 years of data, but do not require a minimum distance this time. The number of stations increases up to
414 around 40 in 1950–1980 and decreases again to the present. On average 1.3 stations are correlated at $r > 1/e$ with
415 each of these stations. We consider the period 1930-2016. The decrease in number of stations at the end implies
416 that a trend in extremes will be negatively biased. The number of events is lower than before (1 per year instead
417 of 19/324 events per year), so the uncertainties are larger.

418 A fit of a time-dependent GEV to the annual and spatial maximum of 3-day averaged precipitation
419 describes the data well (Figure 4). The return time for an event like south Louisiana 2016 anywhere in the
420 Central U.S. Gulf Coast is currently around 30 yr (between 11 yr and 110 yr with 95% C.I.). This is a factor 6.3
421 (C.I. 2.1-50) more than it was in the climate of 1930, corresponding to an increase of intensity of about 25%
422 (C.I. 12%-35%).

423 Analyses of station data analogous to the ones above but for the season July-August-September (JAS)
 424 show somewhat smaller trends, but with larger error margins. The estimated ranges of the JAS analyses and the
 425 all year analyses overlap.



426
 427 **Figure 3:** Fit of the annual maximum 3-day average GHCN-D station precipitation on the Central U.S. Gulf
 428 Coast to a GEV that scales with smoothed global mean surface temperature. (a) Location of all GHCN-D
 429 stations with minimum 10 years of data, (c) observations (blue marks), location parameter μ (thick red line
 430 versus global mean temperature anomalies, relative to 1980-2010), $\mu + \sigma$ and $\mu + 2\sigma$ (thin red lines), the two
 431 vertical red lines show μ and its 95% C.I. for the two climates in (e). (e) Gumbel plot of the GEV fit in 2016
 432 (red line, with 95% uncertainty estimates) and 1900 (blue line), marks show data points drawn twice: scaled up
 433 with the trend to 2016 and scaled down to 1900. The yellow square (line) denotes the intensity of the observed
 434 event at Livingston, LA. (b,d,f) as (a,c,e) but for 19 GHCN-D stations with minimum 80 years of data and
 435 minimum spatial separation of 0.5° .



436

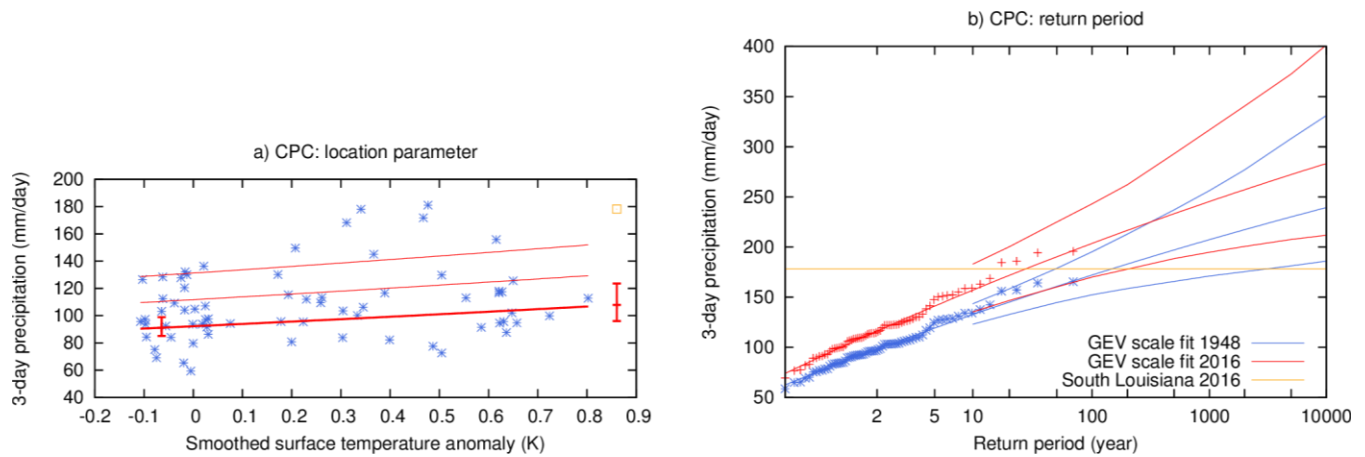
437 **Figure 4:** Fit of the spatial and annual maximum 3-day average GHCN-D station precipitation on the Central
 438 U.S. Gulf Coast to a GEV that scales with smoothed global mean surface temperature. (a) Observations (blue
 439 marks), location parameter μ (thick red line), $\mu + \sigma$ and $\mu + 2\sigma$ (thin red lines versus global mean temperature
 440 anomalies), the two vertical red lines show μ and its 95% confidence interval for the two climates in (b). (b)
 441 Gumbel plot of the GEV fit in 2016 (red line, with 95% uncertainty estimates) and 1930 (blue line), marks show
 442 data points drawn twice: scaled up with the trend to 2016 and scaled down to 1900. The yellow square (line)
 443 denotes the intensity of the observed event at Livingston, LA.

444 3.2 Gridded analysis

445 To compare with the model data, we also analysed the CPC $0.25^\circ \times 0.25^\circ$ gridded precipitation analysis 1948–
 446 2016. Because the spatial extent of 3-day averaged precipitation extremes is larger than the grid boxes, we first
 447 averaged these to a $0.5^\circ \times 0.5^\circ$ latitude-longitude grid. The highest value in 2016 is then 158.77 mm/day, which is
 448 the highest in the record. This is lower than at a single grid point due to the spatial averaging. A GEV fit of all
 449 0.5° grid points (not shown) gives a return time of 550 yr with an uncertainty from 300 to 2000 yr, compatible
 450 with the station analysis but with larger uncertainties. The probability has increased by a factor 3.5 (C.I. 2.0-11)
 451 since 1948, corresponding to an increase in intensity of 15% (C.I. 9%-24%).

452 Taking the spatial maximum of the original $0.25^\circ \times 0.25^\circ$ grid we find that the highest observed value in
 453 2016 is 178.2 mm/day on 12–14 August (534.7 mm in three days). The record is too short to draw robust
 454 conclusions from a fit of a GEV depending on global mean temperature except that the precipitation maxima
 455 also increase in this dataset (Figure 5). In this dataset, the return time for an event like 2016 anywhere on the
 456 Central U.S. Gulf Coast is currently between 9 and 200 yr (best estimate 25 yr). This is about a factor 5 (C.I.
 457 1.1-60) larger than it was around 1948, which equates to an increase in intensity for an event like 2016 of
 458 roughly 15% (C.I. 0.4%-30%).

459 As for station data, analyses of CPC similar to the ones above but for the season JAS show somewhat
 460 smaller trends, but with larger error margins. The estimated ranges of the JAS analyses and the all year analyses
 461 overlap.



462

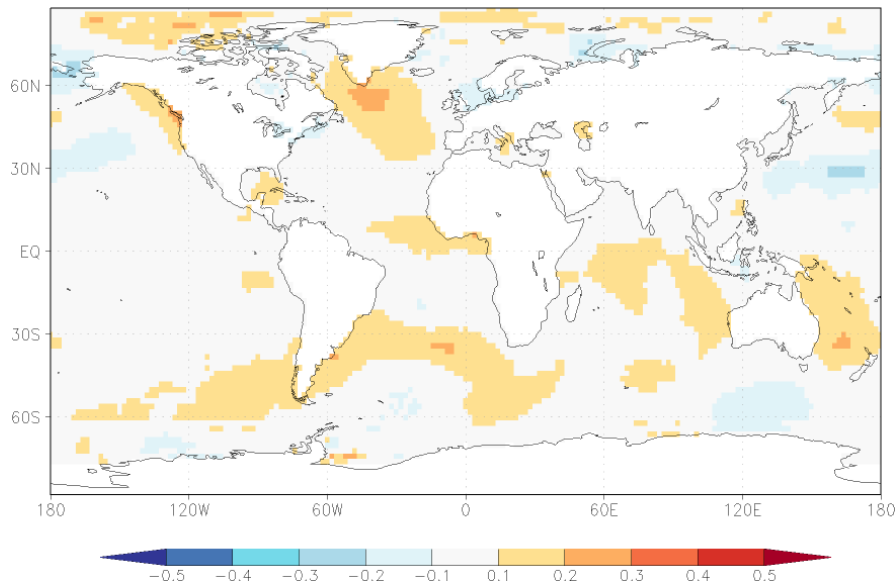
463 **Figure 5:** As Figure 4 but for the spatial and annual maximum 3-day average 1948–2016 $0.25^\circ \times 0.25^\circ$ gridded
 464 CPC analysis.

465 3.3 Influence of natural variability

466 We investigate the influence of natural variability on the probability of an event like south Louisiana 2016 by
 467 using indices of detrended SST as covariates in the time-dependent GEV fits. We first examine the influence of
 468 El Niño-Southern Oscillation (ENSO) by using as a covariate 6-month lagged Niño 3.4-index (5°S – 5°N , 170° –
 469 120°W) minus SST averaged of 30°S – 30°N to remove to first order the effects of global warming. This is
 470 inspired by the heavy rain events after the 1997/98 El Niño event. A comparison of recent Niño 3.4 conditions
 471 with those from a year following the strongest La Niña year (1917) in a fit of all 324 stations with more than 10
 472 years of data suggests that anomalously warm tropical Pacific SSTs significantly ($p < 0.1$) increase the
 473 probability of an event like south Louisiana 2016, but not by much. In the year after El Niño, the probability is a
 474 factor 1.3 (C.I. 1.0-1.9) higher than in a year following a very strong La Niña. However, the maximum of
 475 stations with at least 80 years, which represents the largest events, does not show a signal, albeit with a large
 476 uncertainty of a factor 0.5 decrease to a factor 1.7 increase.

477 Simultaneous correlations with global SSTs indicate a region in the North Atlantic that has a significant
 478 relationship with Central U.S Gulf Coast extreme precipitation at $p < 0.1$ (Figure 6). Although the field
 479 significance is very low, the region is a well-known source of decadal variability and predictability (e.g.,
 480 Hazeleger et al. 2013), so we still consider it a possible source of decadal variability of extreme precipitation.
 481 We use an area-average of SSTs between 45°N – 60°N and 50°W – 20°W as a covariate in the GEV fit. The region was
 482 anomalously cold in 2016, so we compare the changed probability with a warm year (2006). In this statistical
 483 analysis, North Atlantic SSTs are significantly correlated ($p < 0.01$) to Central U.S Gulf Coast precipitation (by
 484 design, as we chose the region that has a significant correlation), with recent below average SSTs decreasing the
 485 probability of an event like 2016 (risk factor 0.37, C.I. 0.11-0.81). To ascertain whether this is a physical
 486 connection and not just a coincidence by picking the region of largest correlations, we need to analyse model
 487 results.

488



489
 490 **Figure 6:** Correlation coefficient between Central U.S. Gulf Coast spatial and annual maximum of 3-day
 491 extreme precipitation intensity and annual mean SST (ERSST v4) with a linear regression on the global mean
 492 temperature removed at each grid point.

493 **4 Model evaluation**

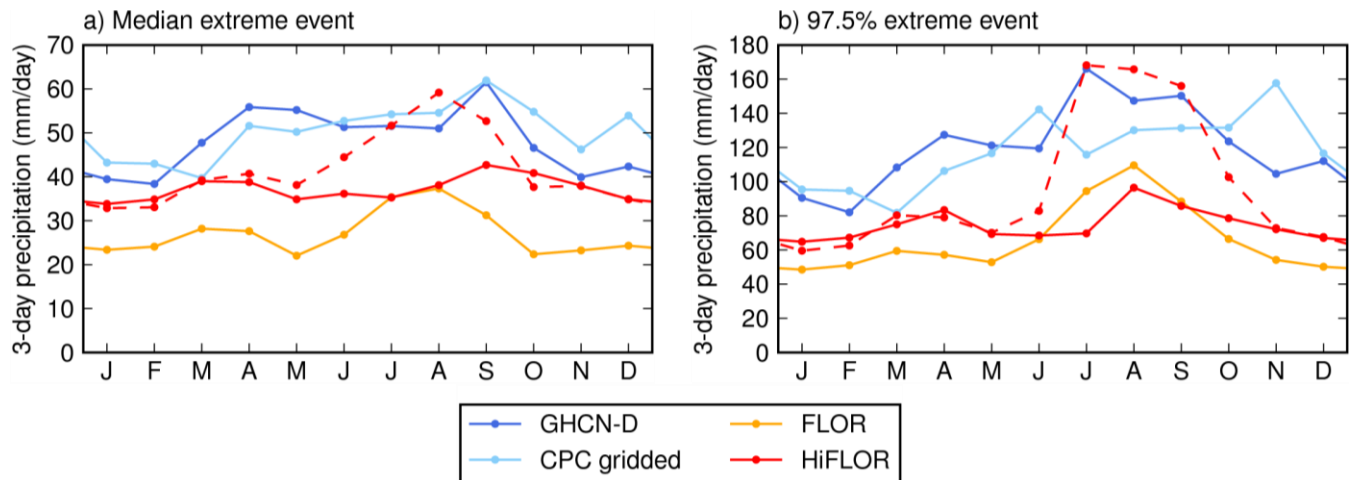
494 We here describe an evaluation of simulated precipitation extremes in the two global coupled models (model
 495 descriptions in Section 2.2). Precipitation is a notoriously difficult field to simulate, as many coupled climate
 496 models exhibit large biases (Dai 2006, Flato et al. 2013). Though FLOR-FA and HiFLOR underestimate the
 497 intensity of Central U.S. Gulf Coast precipitation extremes slightly, this bias is significantly reduced in these
 498 high-resolution models compared to standard-resolution models (Van der Wiel et al. 2016).

499 **4.1 Annual cycle and intensity**

500 First we analyse the annual cycle of extreme precipitation intensity. We consider the median and 97.5 percentile
 501 of the monthly maximum of the spatial maximum of 3-day averaged precipitation (Figure 7). The 97.5
 502 percentile events are of smaller magnitude than the south Louisiana observed event (100-150 mm/day versus
 503 200 mm/day), but we consider smaller magnitude events to increase the number of events in the calculation and
 504 hence decrease uncertainties.

505 The observed precipitation extremes in spring and summer are generally more intense than in autumn
 506 and winter (Figure 7a). There is no agreement between the two observational products on which season sees the
 507 most intense precipitation extremes (97.5 percentile, Figure 7b), though extremes in March-October are more
 508 intense than in winter. This period of stronger extremes is longer than the hurricane season, which provides a
 509 fraction of these extremes. In this region, the models underestimate the intensity of extreme precipitation, which
 510 was also noted in Van der Wiel et al. (2016). FLOR-FA has a peak season for extreme precipitation intensity in
 511 JAS which is not found in the observational data. The HiFLOR SST-restored experiment, in which global SST
 512 biases are decreased compared to the free running experiments, shows a similar peak in JAS. The HiFLOR 1990

513 static forcing experiment however, doesn't show this peak. Instead it has a similar annual cycle structure to the
 514 observational data, though with a smaller amplitude.
 515

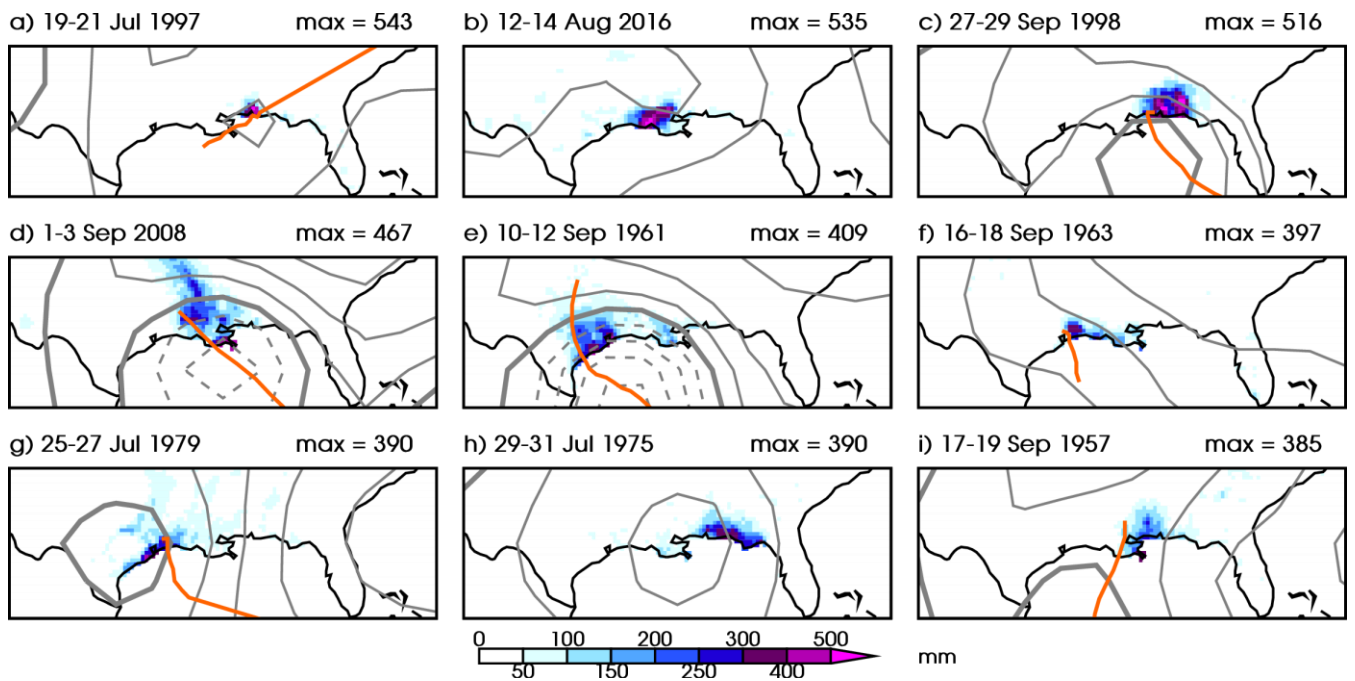


516 **Figure 7.** Annual cycle of monthly and spatial maximum 3-day averaged precipitation for point station data
 517 (GHCN-D, dark blue line), gridded observational data (CPC, light blue line) and model simulations (FLOR-FA,
 518 orange line, and HiFLOR, red lines). For HiFLOR the 1990 static forcing experiment (solid red line) and the
 519 variable forcing SST-restored experiment (dashed red line) are included. Shown are (a) the median value of the
 520 monthly extremes and (b) the 97.5 percentile.
 521

522 4.2 Meteorological conditions

523 Next, we investigate the meteorological conditions generating extreme precipitation events in both models and
 524 compare these to the observed ones. For this analysis we consider the longest static forcing experiments for each
 525 model: 1860 for FLOR-FA and 1990 for HiFLOR and the CPC gridded precipitation analysis. The selection of
 526 these events is limited to the region of interest (Central U.S. Gulf Coast) and the months JAS to facilitate
 527 comparison against the south Louisiana event.

528 Precipitation totals and circulation patterns for the nine largest extreme precipitation events in the CPC
 529 analysis (JAS season only) are shown in Figure 8. Note that the 2016 south Louisiana event ranks as number 2-
 530 heavy precipitation related to Hurricane Danny in 1997 was stronger, though it was confined to a smaller area.
 531 Seven of these nine events were associated with a tropical cyclone/hurricane making landfall (78%, orange
 532 tracks are the International Best Track Archive for Climate Stewardship, IBTrACS, track estimate, Knapp et al.
 533 2010), the exceptions are July 1975 and, as noted before, August 2016. Note that the GEV analysis in Section
 534 3.2 was based on annual maxima, for which the ranked extreme events are different than the ones shown in
 535 Figure 8 (these are nine of the top 14 events when all data is taken into account, ranks 1 and 2 are the same).
 536



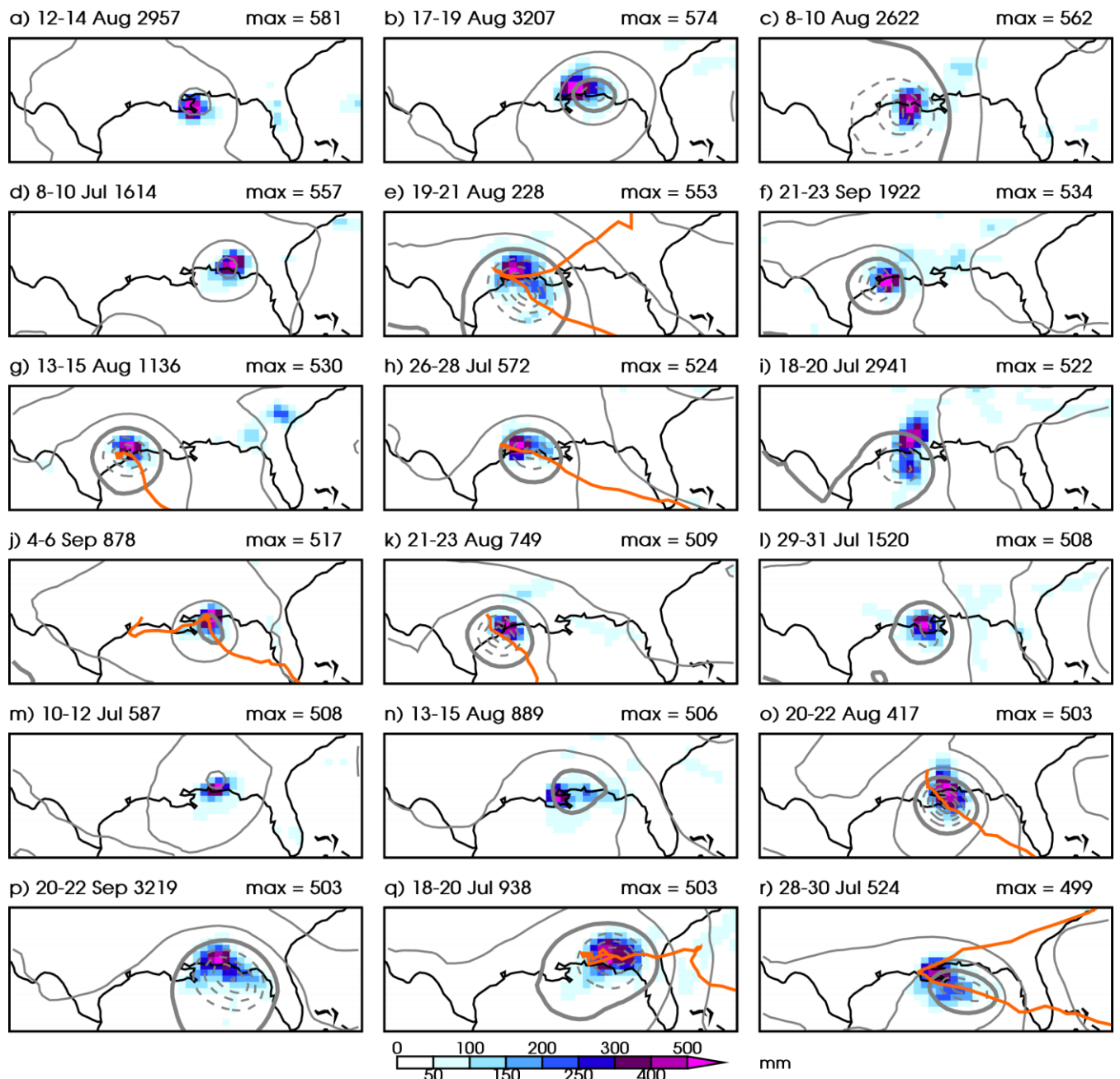
537

538 **Figure 8:** Top 9 extreme precipitation events in the Central U.S. Gulf Coast (29–31 °N, 85–95 °W) for the CPC
 539 gridded precipitation analysis. 3-day precipitation sum (mm, shaded colors, as in Figure 1d), 850-hPa height for
 540 the middle day (grey contours, interval 25 m, 1500 m contour thickened, lower contours dashed) from
 541 NCEP/NCAR Reanalysis 1 (Kalnay et al. 1996) and tropical cyclone track if system is classified as one (orange
 542 line, IBTrACS). These extreme events are calculated for the three month period: JAS.

543

544

545 A similar figure for FLOR-FA is included as Figure 9. We now show the 18 most extreme events
 546 (approximate return period 3530/18≈200 years) in FLOR-FA. The return period in the model for these events is
 547 much larger than the return period for the observed events in the CPC analysis (approximate return period
 548 69/9≈8 years). Despite the negative bias of precipitation extreme intensity (Section 4.1), the precipitation sums
 549 for these events are therefore larger than those in the observed data. All events are associated with a low
 550 pressure system, of which 8 (44%, orange tracks in Figure 9) are a tropical cyclone based on the TC tracking
 551 methodology of Harris et al. (2016) as implemented in Murakami et al. (2015). Note that the low pressure
 552 systems of the top 4 events do not classify as a tropical cyclone, showing the precipitation potential of non-



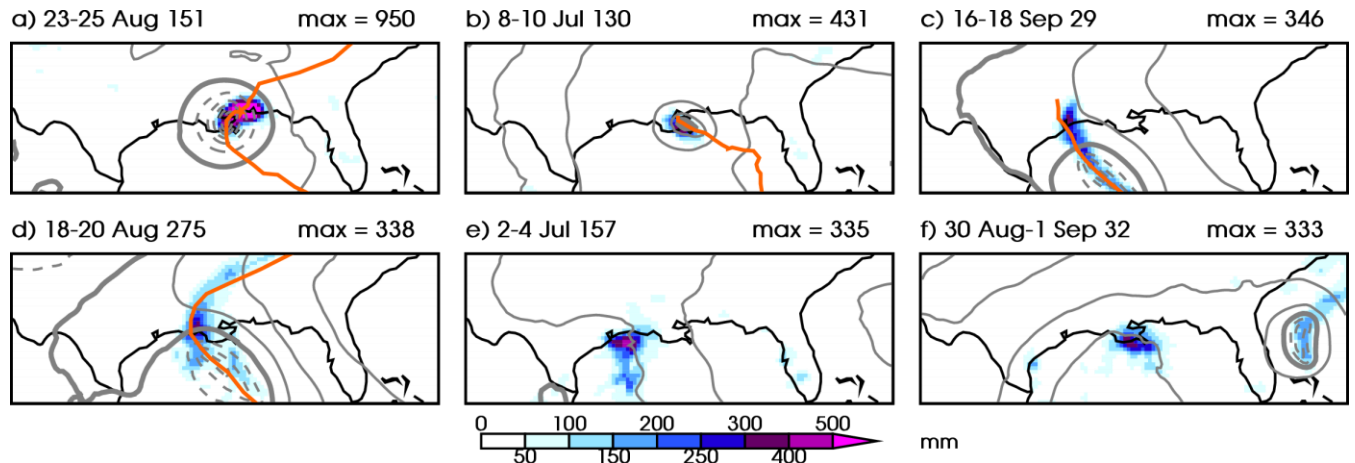
553

554 **Figure 9:** As Figure 8 but for the top 18 maximum extreme precipitation events in the 1860 FLOR-FA static
 555 forcing experiment. Note that years are model years and do not resemble dates on the real world calendar and
 556 that the model provides precipitation information over ocean grid boxes too.

557

558 Because the HiFLOR 1990 static forcing experiment is of smaller length, it is not possible to sample
 559 the 200-year return period event as was done for FLOR-FA adequately. In Figure 10 we show the 6 most
 560 extreme events (approximate return period $280/6 \approx 50$ years, the top 2 events are samples of events with return
 561 periods of about 150 years). In HiFLOR the most extreme precipitation events are the result of a tropical
 562 cyclone, though storm intensity (storms in Figure 10a,b are tropical storms, storms in Figure 10c,d are
 563 hurricanes at the time of landfall) is not related to resulting precipitation magnitude. Note that the strongest
 564 event in HiFLOR exceeds 900 mm over a 3-day period, which is much stronger than the observed values in
 565 south Louisiana.

566 In conclusion, though the precipitation extremes are of smaller magnitude in both models and the
 567 annual cycle in observations is not recovered well (Section 4.1), the meteorological system leading to these
 568 precipitation extremes in JAS are realistic and resemble observed systems (Section 4.2).



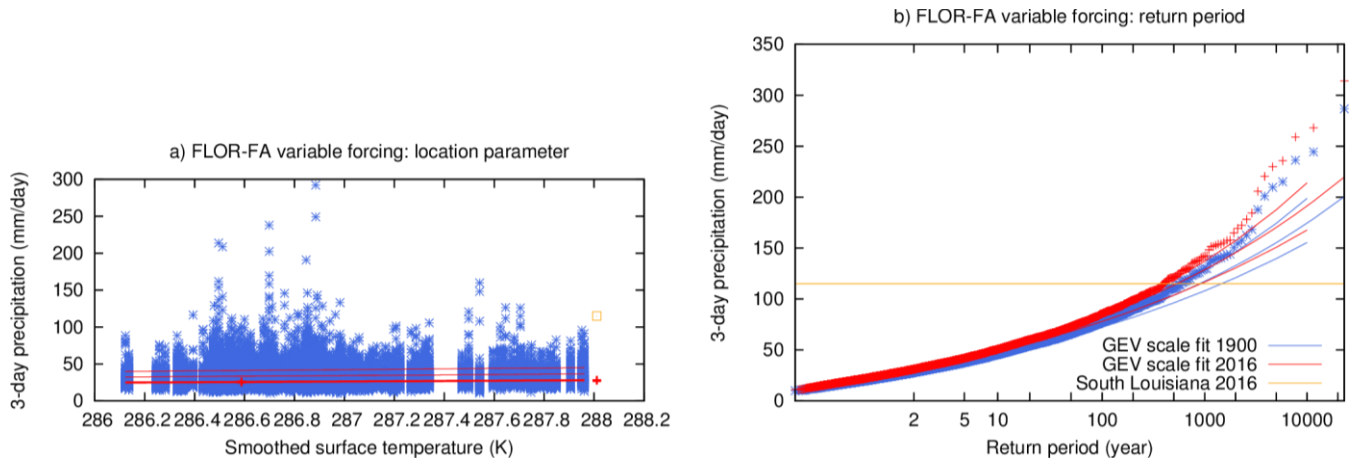
569 **Figure 10:** As Figure 8, but now for the top 6 maximum extreme precipitation events in the 1990 HiFLOR static
 570 forcing experiment. Note that years are model years and do not resemble dates on the real world calendar and
 571 that the model provides precipitation information over ocean grid boxes too.
 572

573 5 Model analysis

574 In order to attribute the observed trend to external forcing we use global climate models that isolate the different
 575 forcings. The model and experimental description can be found in Section 2.2.

576 5.1 FLOR-FA

577 A fit of all land grid boxes ($0.5^\circ \times 0.5^\circ$, 23095 data points) to a time-dependent GEV distribution is shown in
 578 Figure 11. The uncertainties take into account the dependencies by moving spatial blocks of 7.7 grid points on
 579 average. In contrast to the observations (Figure 3) the distribution cannot be described with a single GEV
 580 function: the extremes with return times larger than about 100 years (80 mm/day) diverge from the fit that is
 581 determined mainly by the less extreme precipitation events. This so-called 'double population' problem results
 582 from different meteorological mechanisms for extreme events. We therefore cannot use this fit for attribution.



583
 584 **Figure 11:** As Figure 4 but for the annual maximum 3-day average precipitation in the FLOR-FA variable
 585 forcing experiment (based on complete experiment, 1861-2100).

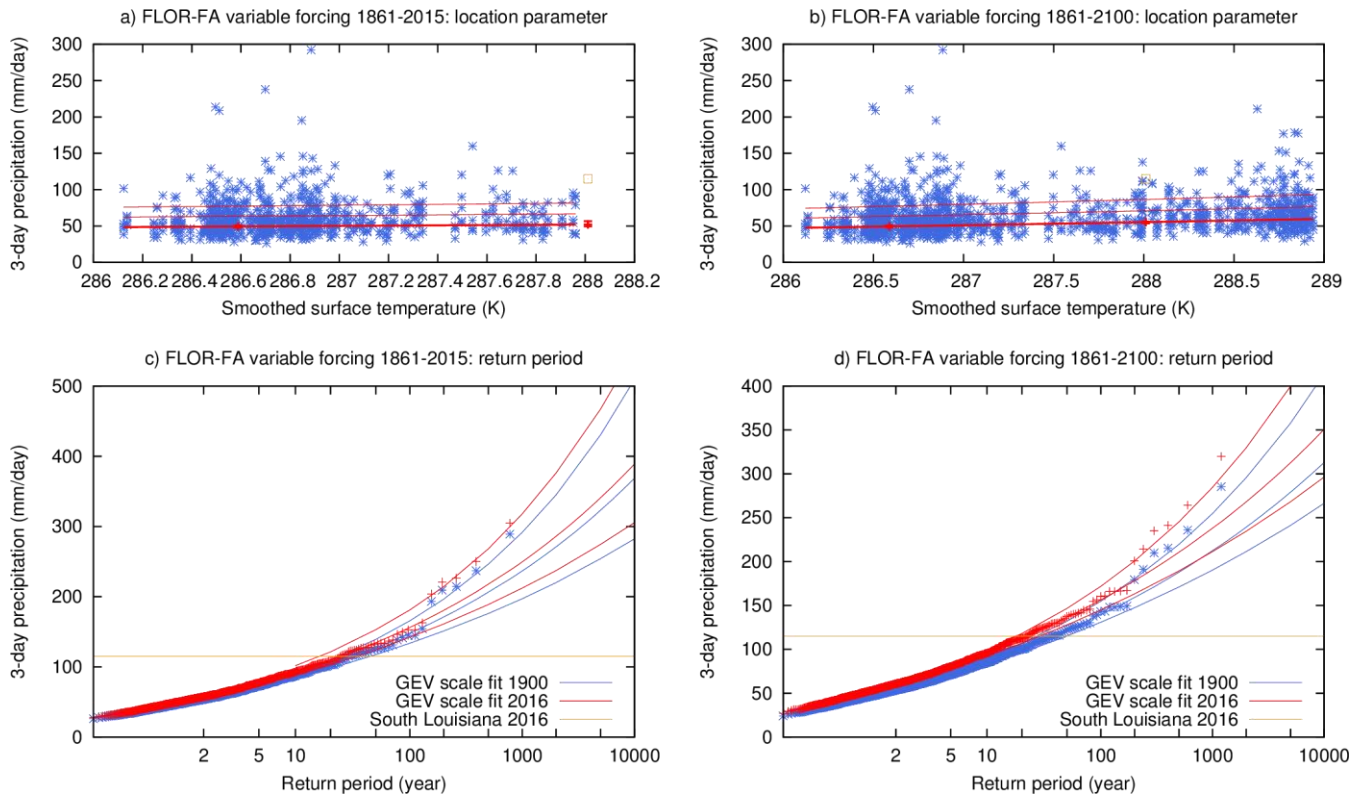
586

587 Taking the spatial maximum of all grid boxes selects only the high end of the distribution. Figure 12a,c
 588 shows the GEV fit to these extremes using data for simulated years 1861-2015. The fit is still not completely
 589 satisfactory as the highest five events (all in the early years of the experiments) fall on the upper boundary of the
 590 95% C.I. around the fit to the rest of the distribution. Due to this, the shape parameter ξ and scale parameter σ of
 591 the GEV distribution are higher than they are in the observations. Because of model bias, we define our event to
 592 have the same return period as the gridded observations in 2016 adjust the model amplitude of extremes to
 593 obtain the same return time as that in observational data, of (around 30 years, (115 mm/day)). This gives a trend
 594 in this model that is significantly greater than zero at $p < 0.05$ (one-sided). However, the factor 1.3 (C.I. 1.0-1.9)
 595 increase in probability, corresponding to an increase in intensity of 5% (C.I. -1%-14%), is much less than the
 596 observed one .

597 Assuming that the relationship with global mean surface temperature does not change in the model
 598 world up to until 2100, in spite of a different mix of anthropogenic forcings (greenhouse gases and aerosols), we
 599 can improve the signal-to-noise ratio of the fit by using all data in the variable forcing experiment (Figure
 600 12b,d). For the spatial and annual maximum of 3-day averaged precipitation this gives an increase in probability
 601 of a factor 1.8 (C.I. 1.4-2.0) corresponding to an increase in intensity of 11% (C.I. 7%-12%) up to now.

602 Analogous analyses but for the season JAS show similar results, although with larger error margins.
 603 We looked for an effect of ENSO in the long static forcing experiment in the same way as in the observations.
 604 This does not show any influence of El Niño averaged over the 12 months July–June preceding the year of
 605 extreme precipitation events.

606



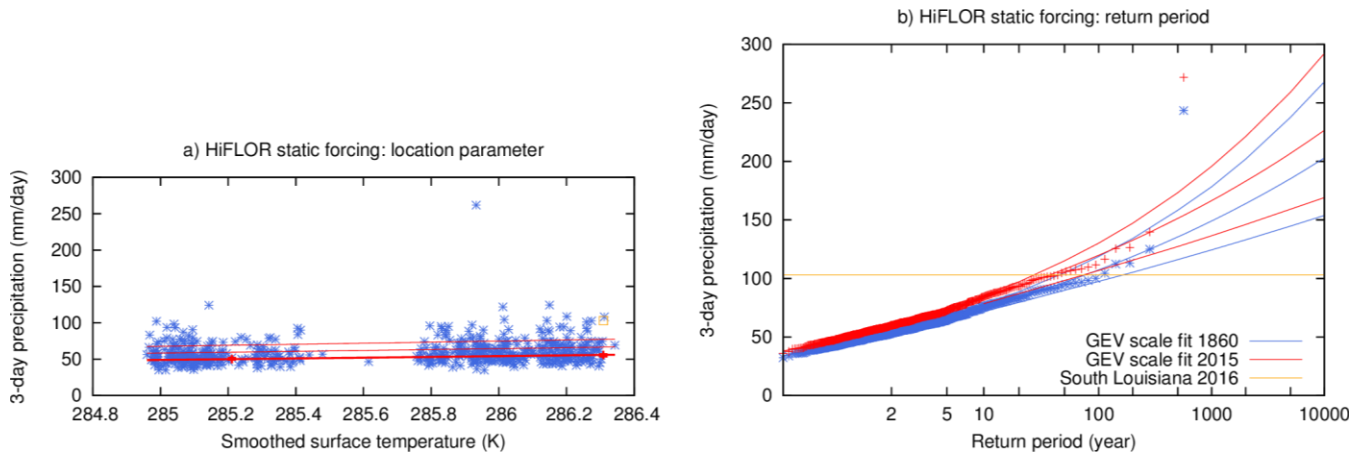
607

608 **Figure 12:** As Figure 4 but for the annual and spatial maximum 3-day average precipitation in the FLOR-FA
 609 variable forcing experiment. (a,c) taking into account years 1861-2015, (b,d) taking into account 1861-2100.

610 **5.2 HiFLOR**

611 The HiFLOR model at a higher 25 km resolution has a more realistic seasonal cycle, but underestimates extreme
 612 precipitation by 25% for a 1 in 1 year event and by 35% for 1 in 1000 year extremes. We correct for this bias ~~by~~
 613 ~~defining our event to have the same return time as the gridded observations in 2016, that is, as we did for the~~
 614 ~~FLOR-FA experiment (the 30 year event is 103 mm/day).~~ We concatenated the four static forcing experiments
 615 that we have available, leaving out the first 20 years of each, to create a 655-year record. To decrease
 616 dependencies we averaged 2×2 grid boxes into a 0.5° grid, this results in each grid box being correlated with
 617 10.3 others with $r > 1/e$ on average.

618 As was found for FLOR-FA, the GEV fit to all grid points results in a double population, therefore we
 619 disregard that analysis and instead focus on the spatial maximum precipitation extreme. Similar for FLOR-FA,
 620 taking the spatial maximum of this 50 km dataset selects mainly events in the more extreme population and does
 621 give a good fit to the GEV distribution (Figure 13). The outlier event is a tropical cyclone in the 1990 static
 622 forcing event, that was discussed in Section 4.2 (Figure 10a). The external forcing, which is the only change
 623 between the static forcing experiments, causes an increase in probability of a 103 mm or stronger event of a
 624 factor 2.0 (C.I. 1.4-2.5), in agreement with the FLOR-FA experiment up to 2100 (Figure 12b,d). This
 625 corresponds to an increase in intensity of 10% (C.I. 5%-12%).



626

627 **Figure 13:** As Figure 4 but for the annual and spatial maximum 3-day average precipitation in the HiFLOR
 628 static forcing experiments.

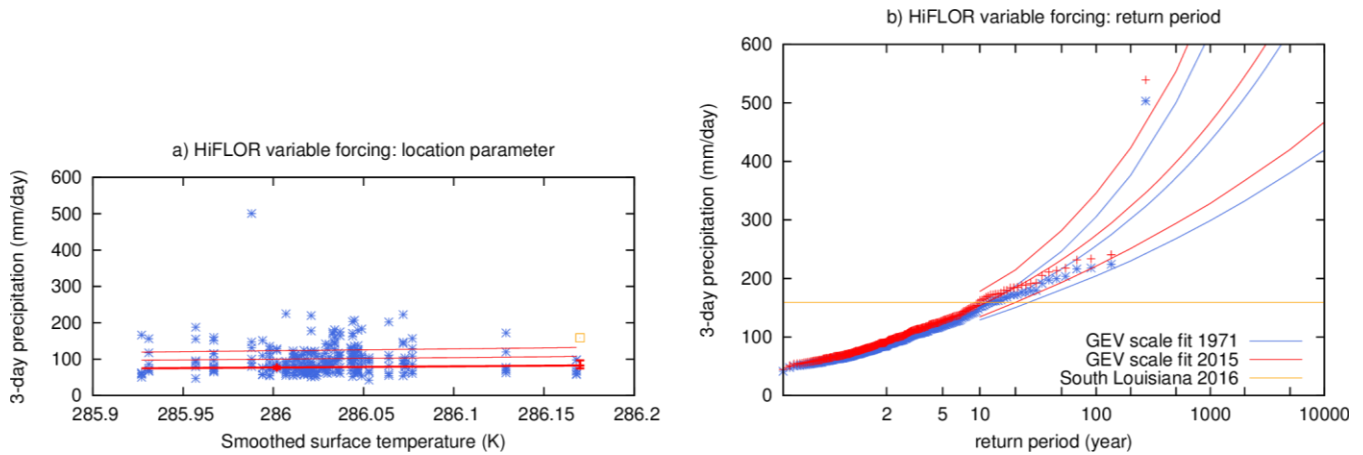
629

630 An analysis of these data using the annual averaged detrended Niño3.4 index lagged by 6 months as
 631 covariate shows a relatively strong influence of El Niño in this model, with an increase in probability from the
 632 year following strongest La Niña to the strongest El Niño of a factor about 4.2 (C.I. 1.7–6.7).

633 We followed the same procedure on the six ensemble members of the variable forcing HiFLOR
 634 experiment (1971–2015). These simulations do not have a negative bias in extreme precipitation. The restored
 635 SSTs eliminate a 2 K cold bias in the subtropical Atlantic that is present in the static forcing experiments, which
 636 may have caused the bias in precipitation extremes on the Central U.S. ~~Central~~ Gulf Coast in those simulations.
 637 Again there is one outlier event with 452.8 mm/day over three days, 1351 mm total.

638 The spatial and annual maximum of 3-day averaged extreme precipitation increases by a factor 1.8
 639 (C.I. 1.2–3.3) in these experiments over the period 1971–2015, corresponding to a change in intensity of 14%
 640 (C.I. 4%–27%), Figure 14. Although the restoring of SSTs increases the fidelity of the simulation, it also
 641 includes the non-forced natural variability of the real world, so these numbers do not isolate the forced change
 642 but show the full change including the effects of natural variability. Assuming these are small compared to the
 643 trend we can extrapolate to the full change since 1900; the period 1971–2015 only includes about 2/3 of global
 644 warming since preindustrial times. This translates to a factor 2.4 (C.I. 1.3–6) increase in probability and 22%
 645 (C.I. 6%–41%) in intensity, which is very similar to the trend found in the observational data.

646 Analyses of the season JAS show similar to somewhat smaller trends, but with larger error margins,
 647 overlapping the all-year error margins.



648

649 **Figure 14:** As Figure 4 but for the annual and spatial maximum 3-day average precipitation in the HiFLOR
 650 variable forcing restored SST experiments.

651 **6 Summary**

652 In this section we summarize the principal observational and model-based results as described in Sections 3 and
 653 5. We have analyzed two observational data products (GHCN-D point station data and CPC 0.25°×0.25°
 654 gridded analysis), to estimate the probability, and changes in probability and intensity of a 3-day precipitation
 655 event as large as that observed in south Louisiana 2015. The analysis was confined to the Central U.S. Gulf
 656 Coast (29–31 °N, 85–95 °W) and relies on time-dependent GEV fits to the data. First we investigated
 657 probabilities and changes at a single station, i.e. the probability of such an event *at a fixed place* in the region.
 658 Second we investigated regional probabilities and changes, i.e. the probability of such an event *anywhere* in the
 659 region. The spatial scale of the most extreme precipitation events is significantly smaller than the region
 660 considered, therefore the second probability is lower than the first. To attribute the observed changes to forced
 661 anthropogenic climate change, we repeat the analysis using high-resolution global climate model data from
 662 GFDL FLOR-FA and GFDL HiFLOR. GEV fits for the local analysis were unsatisfactory, therefore we only
 663 report the regional change in probabilities.

664 The expected return period of a comparable 3-day precipitation event at a single station as high as the
 665 maximum observed is 450 to 1450 year, best estimate 550 year. Return periods like these are often written as a
 666 "1 in 1000 year event". The return time for observing an event anywhere in the region is lower: between 11 and
 667 110 year (best estimate 30 years). All observational analyses found clear positive trends, with an increase in
 668 probability for the regional event of about a factor 6.3 (97.5% certain more than 2.1), and an increase in
 669 intensity of 12% to 35% (Table 3). Estimates based on CPC gridded data are comparable but have larger ranges
 670 due to the shorter period of data availability.

671 **Table 3:** Summary of observed (first two rows) and modeled (third row and down) changes in regional rainfall
 672 extremes in Central U.S. Gulf Coast. Note the modeled changes can be attributed to anthropogenic climate
 673 change.

Data source (years used for calibration)	Baseline regional return period for 2016 event (95% confidence range, observations only)	Years change calculated over	Change of return period in present day over given years (95% confidence range)	Change in intensity of regional 30- year return event in 2016 since beginning of record (95% confidence range)
GHCN-D rain	30 year (11 - 110)	1930-2016	6.3× (2.1 ... 50)	+25% (12% ... 35%)

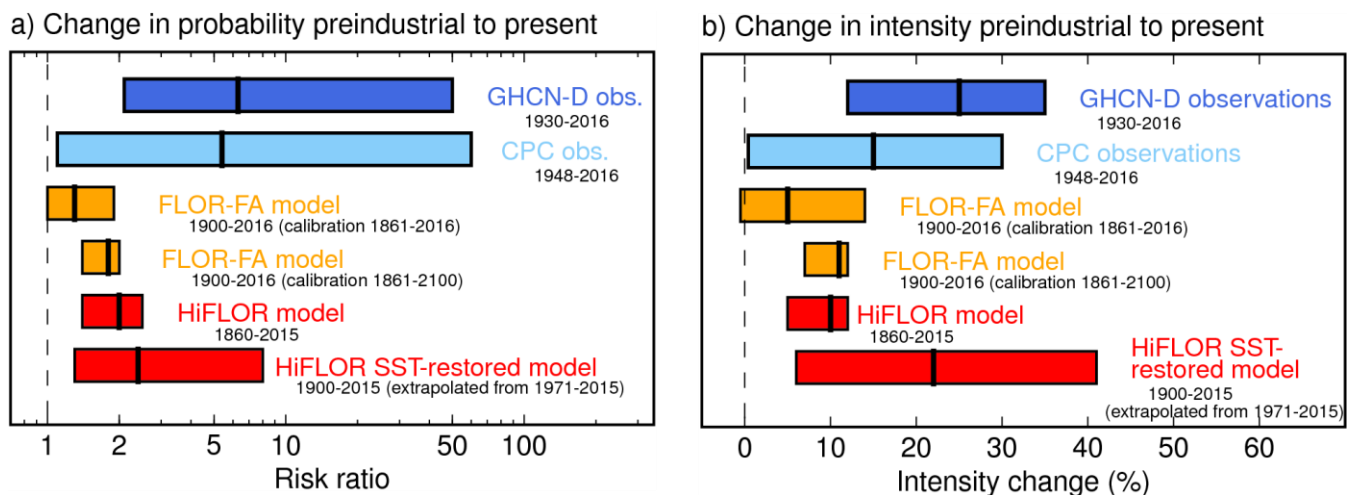
gauges, minimum 80 year data (1930- 2016)				
CPC 0.25°×0.25° gridded data (1948-2016)	25 year (9 - 200)	1948-2016	5.4× (1.1 ... 60)	+15% (0.4% ... 30%)
FLOR-FA variable forcing experiment (1861-2015)		1900-2016	1.3× (1.0 ... 1.9)	+5% (-0.5 ... 14%)
FLOR-FA variable forcing experiment (1861-2100)		1900-2016	1.8× (1.4 ... 2.0)	+11% (7% ... 12%)
HiFLOR static forcing experiment (1860, 1940, 1990, 2015)		1860-2015	2.0× (1.4 ... 2.5)	+10% (5% ... 12%)
HiFLOR variable forcing experiment (1971-2015), extrapolated to 1900-2015		1900-2015	2.4× (1.3 ... 8)	+22% (6% ... 41%)

674

675 The sensitivity of precipitation extremes from both models is consistent with that estimated from the
676 gridded observations. The lower-resolution FLOR-FA model shows lower trends than the HiFLOR model. For
677 the HiFLOR model the sensitivity estimated from the SST-restored experiment for 1971–2015 is larger than that
678 from the coupled simulations. Taking into account all modeling results, the probability of an event like south
679 Louisiana 2015 has increased at least by a factor 1.4 due to radiative forcing; the two HiFLOR experiments and
680 the analysis of the full dataset from FLOR-FA suggest central values close to a doubling of probability. Such an
681 increase may be translated to what was once a 1/100 year event somewhere in the Central U.S. Gulf Coast,
682 should now be expected to occur on average, at least once every 70 years, likely even more common. This trend
683 is expected to continue over the 21st century as past and projected future greenhouse forcing continues to warm
684 the planet.

685 The evidence for an influence of the strong 2015/2016 El Niño increasing the probability of the 2016
686 event is equivocal. The full station dataset shows a statistically significant but small increase in probability, but
687 we do not find the same for the spatial maximum, which represents the strongest events. The FLOR-FA model
688 similarly does not have an ENSO effect, whereas the HiFLOR model again shows a higher probability after a
689 large El Niño. We have found some evidence for decadal Atlantic variability affecting precipitation in the
690 observations, which would have decreased the likelihood in 2016 if confirmed.

691



692

693 **Figure 15:** Summary of observed (GHCN-D, CPC, blue colors) and modeled (FLOR-FA, HiFLOR, yellow, red
 694 color) changes in regional precipitation extremes in Central U.S. Gulf Coast. Ranges written in black are the
 695 time periods for which the change is shown over. Calibration for the calculations is done over separate time
 696 periods for noted models. See Table 3 for specific numeric values.

697 7 Discussion

698 We have presented a rapid attribution to climate change and climate variability of the south Louisiana intense
 699 precipitation event. Here we lay out the crucial assumptions made to conduct our assessment, further lines of
 700 inquiry to investigate the validity of the crucial assumptions and the sensitivity of our results to changes in these
 701 assumptions, suggestions for further study on related topics not investigated here, and questions that arise from
 702 this work. Finally, we note some societal impacts ~~and management implications~~ of the findings.

703 7.1 Crucial assumptions

704 In performing these analyses, we have made the following crucial assumptions about ~~the observations, models,~~
 705 the statistical distribution of precipitation extremes, ~~the observations ,and~~ the relationship between temperature
 706 and precipitation extremes, ~~and the models~~. We have tested the sensitivity of our results to some of these
 707 assumptions in the results sections (Sections 3-5) and discuss them below.

- 708 1) We assume that the local, annual maxima of 3-day averaged precipitation over the region of analysis
 709 (29–31 °N, 85–95 °W) can be grouped together, and that their statistical distribution follows a GEV
 710 distribution. Underlying this assumption is that the region has homogeneous extreme precipitation
 711 characteristics (Figure 1f). Furthermore, we assume that all the annual maxima of 3-day averaged
 712 precipitation are drawn from the same statistical distribution, in spite of the many different mechanisms
 713 that lead to extreme precipitation in this region, and that this distribution can be represented well by a
 714 GEV distribution. We further assume that the spatial maximum over the region can also be described
 715 by a GEV.
- 716 2) We assume that analyzing all seasons together provides a fuller distribution of the population of
 717 extreme precipitation events than isolating the analysis to seasons proximate to August (the month in
 718 which the south Louisiana event occurred). In part, the choice to analyse annual extreme events was
 719 motivated by the fact that a variety of meteorological phenomena can lead to extreme precipitation in

720 this region, flooding can occur in any season, and precipitation extremes may change in various
721 seasons (Lehmann et al. 2015, Van der Wiel et al. 2016). All extreme value analyses were repeated
722 focusing only on the JAS season and the qualitative nature of the results was the same as those
723 presented.

724 3) We assume that the inhomogeneities in point station data due to station changes, incomplete records
725 and geographic coverage are smaller than the trends and have no coherent sign. We have checked this
726 by performing the analysis on all stations and for a subset of stations with long (at least 80 year)
727 records and sufficient (0.5°) spatial separation.

728 4) We assume that the methods that create the gridded observationally-based precipitation data result in
729 an accurate representation of 3-day average precipitation at the grid scale. The decorrelation scale of 3-
730 day precipitation is about twice the grid scale, so the largest uncertainty is the inhomogeneous
731 distribution of the gauge stations in space and time. A comparison of the results with point station data
732 shows that the differences are not large.

733 5) We assume that, for the assessment of trends in GEV statistics, global mean surface temperature
734 represents a relevant covariate to capture the *a priori* expected connection between precipitation
735 extremes and temperature (e.g., O’Gorman 2015). A physical motivation for this expected connection
736 is the dependence of the saturation specific humidity of air on temperature through Clausius-Clapeyron
737 (see Section 1). The underlying assumption is that multi-decadal temperature changes exhibit “pattern
738 scaling”, such that global mean temperature change is a sufficient parameter to describe the long-term
739 changes of temperature; furthermore, global-mean temperature helps increase the signal-to-noise ratio
740 of fits to temperature changes. If there is substantial spatial heterogeneity to temperature changes on
741 multi-decadal timescales, the assumption that global mean temperature is the relevant metric becomes
742 suboptimal. Furthermore, if dynamical changes (e.g., changes in the statistics of storms, changes in the
743 dominant moisture sources for extremes, etc.) dominate the observed multi-decadal precipitation
744 extreme changes, this assumption will also be suboptimal.

745 6) We assume that the probability density function of precipitation extremes scales with a covariate, for
746 example (smoothed) global mean temperature and does not exhibit other changes in shape. This
747 assumption is supported by large-sample statistics from modelling experiments such as
748 Weather@Home (Massey et al. 2015) in other regions, but it is not *a priori* obvious that these results
749 should also hold for the Central U.S. Gulf Coast with its wide variety of weather phenomena causing
750 extreme precipitation. Furthermore, the Massey et al. (2015) results were from models of resolution too
751 low to resolve many of the meteorological phenomena that lead to extreme precipitation (e.g. tropical
752 cyclones) in this region.

753 7) We assume that, beyond an initial rapid (~20 year) adjustment to different static radiative forcings, the
754 statistics of precipitation extremes in the static forcing model experiments depend on global mean
755 temperature in the same way as the changes arising from slow drift due to top of the atmosphere
756 radiative disequilibria and slow ocean adjustment. The latter changes are smaller than the forced trend,
757 so the impact of slow model drift on the results is small.

758 8) We assume that the CMIP5 historical forcings (1860-2005) and RCP4.5 forcings (2005-2100), as
759 implemented in the models, are sufficiently accurate representations of the actual changes in radiative

760 forcing that occurred in the real climate system to allow meaningful comparison of modeled changes in
761 precipitation extremes to those observed.

762 9) We assume that the FLOR-FA and HiFLOR modeled responses to changes in radiative forcing are
763 meaningful estimates of the sensitivity of precipitation extremes in the real climate system, since these
764 models capture multiple physical factors affecting precipitation extremes in a physically-based and
765 internally-consistent framework. This assumption is motivated in part because of the ability of these
766 models to simulate large-scale precipitation and temperature over land (e.g., Van der Wiel et al. 2016;
767 Delworth et al. 2015; Jia et al. 2015, 2016), precipitation extremes over the U.S. (Van der Wiel et al.
768 2016), modes of climate variability (e.g., Vecchi et al. 2014; Murakami et al. 2015); the meteorological
769 phenomena that lead to precipitation extremes and their relationship to modes of climate variability
770 (e.g., Vecchi et al. 2014; Krishnamurthy et al. 2015; Murakami et al. 2015, 2016; Zhang et al. 2015,
771 2016; Pascale et al. 2016); and that these models show skill at seasonal predictions of large-scale
772 climate, regional hydrometeorology and the statistics of weather extremes across a broad range of
773 climatic regimes (e.g., Vecchi et al. 2014; Jia et al. 2015, 2016; Yang et al. 2015; Msadek et al. 2015;
774 Murakami et al. 2015, 2016). However, it is important to note that climate models can show a range of
775 global and regional climate sensitivities to changing radiative forcing (e.g., Kirtman et al. 2013, Collins
776 et al. 2013)

777

778 These assumptions were crucial to enable a rapid assessment of the climate context of the extreme
779 precipitation of the August 2016 south Louisiana event. Subsequent analyses should further assess the validity
780 of these assumptions, and the quantitative impact of failures in their validity. Below we outline our present
781 evaluation of the implications of these choices and potential areas of further research.

782 Sensitivity experiments should be produced by varying the parameters of our study. We did not
783 conduct analysis of how the size of our defined box for the Central U.S. Gulf Coast affects our results (crucial
784 assumption 1). If the region is altered to remove points that have greater risks relative to those included, the
785 findings may change. Changes in extreme precipitation risks in the Central U.S. Gulf Coast should not be
786 applied elsewhere without further investigation. Temporally, we were able to validate the seasonal distribution
787 of precipitation extremes in models and observations (Section 4.1), and redid the analysis for JAS only, which
788 gave larger uncertainties and somewhat smaller trends (crucial assumption 2). Future work could further
789 quantify seasonal differences in extremes and their response to climate forcing. Similarly, to sample the spread
790 in sensitivity to future RCP forcings (crucial assumption 8, used for any modeled years beyond 2005), our
791 results may be revised with different climate forcings. For the near term however, this is likely not an issue in
792 HiFLOR (used to produce climates for 2005-2015 in the static forcing and nudged SST runs) as climate
793 variability tends to be greater than the climate response to different scenarios during this time period (Forster et
794 al. 2013; Hawkins and Sutton 2009; Kirtman and Power 2013), but may affect future climate results in the
795 FLOR-FA variable forcing experiment at the end of the century (2100, Hawkins and Sutton 2009).
796 FinallyFurthermore, the appropriateness of GEV fits in general should be tested (crucial assumptions 1,6).

797 Sensitivity experiments of our results to model bias and integration length (or length of the observed
798 record) should be produced (crucial assumptions 3 and 7). Short records limit the reliability of the statistics of
799 precipitation extremes. This is important for our model validation of the annual cycle of extremes (Section 4.1)

800 and for the comparison of modeled and observed GEV fits (Section 5). The statistics of precipitation extremes in
801 HiFLOR are closer to those observed than the statistics in FLOR-FA. However, we note that the model
802 experiments with FLOR-FA are significantly longer and therefore provide better statistics of its (biased) climate
803 than the experiments with HiFLOR or the observed record. It cannot thus be fully-excluded that the double
804 distribution of extremes in FLOR-FA or the large peak in JAS in extreme precipitation intensity is purely a
805 result of model bias.

806 A portion of the beginning of the static forcing experiments have been disregarded to allow the model
807 to spin-up in response to radiative forcing. GEV fits were originally calculated by disregarding the first 10 years
808 of data to allow for spin-up, but was extended to 20 years to provide the simulated climate more time to
809 approach equilibrium (crucial assumption 7). The results are only altered slightly by this sensitivity test. Given
810 the length of the available ensemble suite of static forcing experiments, disregarding more years in the
811 beginning of the simulation would reduce our ability to sample extremes. With longer integrations of static
812 forcing experiments and additional ensemble members, we would have more information to assess how model
813 spin-up may affect our results. Similarly, longer integrations would allow for an assessment of the impact of
814 model drift due to ocean adjustment (crucial assumption 7).

815 The attribution to climate change presented here depends on our assumption that changes in
816 precipitation extremes scale with global mean temperature and do not arise from changes in the shape of their
817 underlying distribution (crucial assumptions 5 and 6). The thermodynamic basis of this assumption is based on a
818 large body of research (O’Gorman 2015), however as noted before there is a large variety of synoptic systems
819 that may cause precipitation extremes in the Gulf Coast region. It is not obvious that possible impacts of
820 changes in synoptic weather patterns scale with global mean temperatures. For example, the frequency, track
821 location and/or intensity of tropical cyclones (responsible for 7 out of the 9 most extreme events in JAS were
822 related to tropical cyclones, Figure 8) can each change in complex ways that need not scale with each other or
823 global mean temperature (e.g., Vecchi and Soden 2007; Murakami and Wang 2010; Emanuel and Sobel 2013;
824 Emanuel et al. 2013; Knutson et al. 2013; Vecchi et al. 2013; Walsh et al. 2015), and could cause changes to the
825 statistics of extreme rainfall in the Central U.S. Gulf Coast. Further research must investigate what the impact of
826 dynamic changes (e.g. frequency of occurrence of various synoptic systems, dominant moisture sources,
827 precipitation efficiency) is on the presented trend of precipitation extremes.

828 To investigate the sensitivity of the results to the chosen observational data sets (both based on rain
829 gauge measurements, crucial assumption 3 and 4), we suggest repeating the current analysis with an
830 independent observational estimate of current and historical precipitation along the Gulf coast (e.g. estimates
831 based on satellite data). Furthermore, though we use two global climate models (FLOR-FA and HiFLOR,
832 crucial assumptions 7 and 9) and various experimental setups (static radiative forcing, time-varying radiative
833 forcing and restoring observed SST variability), the models are part of the same NOAA/GFDL family.
834 Consequently, they exhibit similar patterns of (surface temperature) bias and rely on the same parameterization
835 schemes for precipitation. Further inquiry for understanding model-specific biases that may impact the results
836 may still be warranted. For example, there is a North Atlantic cold bias in the models, thought to be connected
837 in part to inadequate eddy parameterizations and a resulting cloud feedback (Delworth et al. 2006; Delworth et
838 al. 2012; Vecchi et al. 2014; Murakami et al. 2015). This may be the source of higher magnitudes of modeled
839 extreme precipitation found due to climate variability in the HiFLOR restored-SST experiments. An assessment

840 using different climate models would therefore add value to allow for a sampling of risk across models, in
841 addition to across experimental setups. These will be available shortly in the HighResMIP project (Haarsma et
842 al. 2016).

843 **7.2 Future work and broader impacts**

844 As described in the introduction and methods, we have purposefully focused our present assessment on
845 one aspect of the flooding problem: the risk of extreme precipitation events that have the potential to produce
846 inland flooding. We have provided provisional streamgauge data in the introduction (Figure 2) to illustrate the
847 effect of the August 2016 event, but have not examined flood risks in the region from streamgauge data directly.
848 Part of the reason for this is that real-time streamgauge data is provisional and subject to revision, which can be
849 exacerbated during a flood when gauges can be overtopped and have missing data due to high water volumes or
850 streamgauge malfunctions (Rantz 1982). The USGS advises users to cautiously consider the use of provisional
851 streamgauge data for decision making (official USGS provisional policy available:
852 <<https://water.usgs.gov/wateralert/provisional/>>). A complimentary modeling study of land surface conditions
853 and interactions with the river environment also requires a more local modeling approach, potentially with a
854 hydrologic model with information on the river system and small scale water processes, and conceivably
855 including an estimate of the impact of direct human impacts (through urbanization, water diversion and
856 management, etc.) which under our time constraints, data access, and present capabilities of our climate models
857 was not feasible.

858 It is important to distinguish extreme precipitation events that are the topic of this study, motivated by
859 the August 2016 rain event that led to devastating “freshwater” or “inland” flooding in south Louisiana, from
860 events that lead to “coastal” or “saltwater” flooding. In particular, the climate change context of saltwater
861 flooding must include an assessment of the regional sea level change contributions and meteorological
862 conditions that can influence these types of events (e.g., Katsman et al, 2008, Sterl et al, 2012, Lin et al. 2012,
863 2014, Little et al. 2014). While certain meteorological conditions, such as landfalling tropical cyclones, can lead
864 to both freshwater and saltwater flooding (e.g., Lin et al. 2012, Villarini et al. 2014), the assessments and
865 discussions presented here are only relevant to extreme rainfall events that have the potential to initiate inland
866 flooding; we do not address changes in storm surges, nuisance flooding (Moftakhari et al. 2015) or other
867 saltwater flooding events.

868 Dependence of the statistics of extreme precipitation events in the Central U.S. Gulf Coast on large-scale
869 climate drivers could provide a scientific basis for seasonal predictions of the odds of these events, much as is
870 now regularly done for the statistics of hurricanes. However, as we show in Section 3.3, we are unable to find
871 strong connections between the statistics of these extreme precipitation events and modes of SST variability
872 (e.g., ENSO), which suggests the possibility for limited seasonal predictability for these events beyond the
873 multi-decadal increase in probability from long-term climate warming. However, potential sources of
874 predictability may be uncovered by future refined analyses.

875 The extent to which the changing risk of extreme rainfall events like that in south Louisiana has
876 implications for stakeholders, such as homeowners, local and federal governments, the humanitarian system,
877 and the insurance industry, will depend on details of the exposure, vulnerability and the disaster preparedness
878 and response strategies available to each. Changes to the physical system are a key factor in adaptation and

879 decisions, but these factors operate in a complex landscape. Through a disaster management lens, the increased
880 frequency of this type of event found in this study may place strains on humanitarian responders and
881 institutions, ~~especially in the future if this type of extreme event continues to become more frequent now and in~~
882 ~~the future~~. Knowing the change in return periods of the most extreme events can help to provide insight into
883 how humanitarian institutions can evolve to be prepared for the future; in addition to adapting to a broader trend
884 of increasing hydro-meteorological disasters globally (CRED 2015). A worthwhile topic to explore in further
885 assessment of this and related events is the extent to which public and media perception both before (local
886 preparedness, willingness to evacuate) and after (nationwide media coverage and awareness of impacts) may
887 have been impacted by the fact that the storm was not named. However, there is an insufficiency of peer-
888 reviewed literature on this topic, even as media outlets in the UK and U.S. have started naming winter storms
889 following the German example (Cutlip 2013, Van Oldenborgh et al. 2015).

890 It is essential to note that this analysis has pursued an assessment of the climate change context of
891 extreme precipitation events (a “climate attribution” study) in which we evaluate the impact of climate
892 conditions and changes in radiative forcing on the probability of extreme rainfall events in south Louisiana and
893 the Central U.S. Gulf Coast. This analysis is fundamentally different in nature from (and complementary to)
894 assessments of the synoptic chain of events that led to the particular Louisiana extreme precipitation event in
895 August 2016 (we would label that “synoptic attribution”). Synoptic attribution of the event generally involves a
896 clear chain of events that led to the extreme rainfall event in a relatively deterministic fashion. Meanwhile, the
897 climate attribution presented here is fundamentally probabilistic. Although we recognize that the synoptic
898 context of this particular extreme event is unique (in fact all events are unique in detail), we have sought to
899 understand the climate context of the probabilities of a class of events that causes extreme precipitation in the
900 Central U.S. Gulf Coast of which this event (flood-inducing extreme precipitation in south Louisiana) is a
901 member (Otto et al, 2016). Furthermore, it is possible to assess the climatic context in more detail, by assessing
902 more proximate climate drivers than global-mean temperature or radiative forcing (e.g., by looking at the impact
903 of particular patterns of SST), or by a more refined assessment of the detailed impact of the superposition of
904 modes of climate variability and multi-decadal climate change (e.g., Delworth et al. 2015, Jia et al. 2016). For
905 any particular event a spectrum of attribution studies (from purely synoptic to purely climate) could, and
906 perhaps should, be pursued in order to unravel the various factors relevant to that event. Moreover, some of
907 these studies are feasible at rapid attribution timescales while others require more time and focused resources to
908 produce the specific and targeted modeling experiments and observational analyses.

909 ~~Our ability to perform the climate attribution of this event was made possible by~~ Climate attribution
910 studies such as this one can only be performed with pre-existing multi-centennial global simulations with high
911 spatial resolution models, ~~which~~ This allowed us to efficiently assess the impact of radiative forcing changes
912 on regional extreme precipitation events. These simulations, obviously, necessitated the long-term research
913 aimed at developing these high-resolution models (e.g., Putnam and Lin 2007, Delworth et al. 2012, Vecchi et
914 al. 2014, Murakami et al. 2015). Furthermore, this work was enabled by a body of work using these models that
915 provided the necessary understanding of the characteristics and fidelity of these models to simulate large-scale
916 and regional climate, and weather events over a broad range of scales and phenomena (e.g., Vecchi et al. 2014;
917 Msadek et al. 2014; Delworth et al. 2015; Jia et al. 2015, 2016; Murakami et al. 2015, 2016; Krishnamurthy et
918 al. 2015; Zhang et al. 2015, 2016; Pascale et al. 2016; Van der Wiel et al. 2016).

919 In particular, this paper follows on a recent analysis of the climatology and CO₂ sensitivity of extreme
920 precipitation events over the U.S. in these same models, showing that FLOR and HiFLOR in particular are
921 uniquely capable of capturing Central U.S. Gulf Coast precipitation extremes, which has large biases in coarser
922 resolution models (Van der Wiel et al. 2016). Though the analysis of extreme precipitation events in Van der
923 Wiel et al. (2016) is of a different nature (focusing on much lower return period events, using different statistical
924 methods, and focusing at the grid point scale rather than regional events), the results presented there are
925 consistent with the current analysis. The previous paper showed that in response to increasing CO₂ levels in the
926 atmosphere, precipitation extremes along the Central U.S. Gulf Coast increase in intensity, with less likely
927 events exhibiting larger fractional intensity increases.

928 We have here sought to provide a scientifically rigorous rapid assessment of the climate context of this
929 precipitation event, which had tragic consequences, to provide meaningful grounding to the public discussions
930 of this event, given both the intense interest in this specific event and our ongoing work on the general subject of
931 climate and extremes (and precipitation extremes in the U.S. in particular, Van der Wiel et al. 2016). We hope
932 that this study, including our explicit discussion of the assumptions needed to pursue this accelerated
933 assessment, will help push the scientific conversation forward to improve our understanding of the risks and
934 return periods of extreme precipitation in the Central U.S. Gulf Coast. The field of rapid attribution analysis is
935 still nascent and may one day lead to such assessments being the normal course of action in response to an
936 extreme event to help provide scientific basis for real-time discussions, and in longer-term disaster response and
937 rebuilding. Until that time, studies such as this will likely only be done for select regions and event types where
938 there is sufficient easily accessible data, and a team of scientists with the necessary expertise and ability to make
939 time in their schedules to provide a rapid assessment. We expect that these early efforts at event attribution will
940 expand our knowledge and capabilities on this subject, and facilitate further inquiry.

941 **Acknowledgements**

942 We thank Geert Lenderink, Sarah Kew, Nathaniel Johnson, Kieran Bhatia and Fanrong Zeng for their helpful
943 comments on an earlier version of the manuscript. Funding for this work was supplied by the National Oceanic
944 and Atmospheric Administration, U.S. Department of Commerce to the Geophysical Fluid Dynamics
945 Laboratory, to the Cooperative Institute for Climate Science (award NA14OAR4320106). The statements,
946 findings, conclusions, and recommendations are those of the authors and do not necessarily reflect the views of
947 the National Oceanic and Atmospheric Administration, or the U.S. Department of Commerce, or other affiliated
948 institutions. This project was made possible through generous support from donors to Climate Central's World
949 Weather Attribution initiative and the EU project EUCLEIA under Grant Agreement 607085. CPC U.S. Unified
950 Precipitation data provided by the NOAA/OAR/ESRL PSD, Boulder, Colorado, U.S. and can be downloaded
951 from: from <http://www.esrl.noaa.gov/psd/>. USGS data was obtained from the automated website and are
952 provisional and subject to revision. The data are released on the condition that neither the USGS nor the United
953 States Government may be held liable for any damages resulting from its use.

954 **Data availability**

955 NOAA GFDL climate model data is not readily available globally at all grid points and for all simulations
956 owing to the size of daily global climate model output for high resolution models with thousands of years of

957 simulations (on the order of 100x terabytes). We have made the precipitation data for the Central U.S. Gulf
958 Coast, global temperature and ENSO data that were used in this study available at the Climate Explorer:
959 <http://climexp.knmi.nl/selectfield_att.cgi>.

960 **References**

- 961 Allen, R. and Burgess, R.: LSU AgCenter predicts floods cost state at least \$110 million in crop loss. The
962 Advocate, viewed 26 August 2016. <[http://www.theadvocate.com/louisiana_flood_2016/article_a7689806-
963 6946-11e6-a681-ab59c458f55c.html?sr_source=lift_amplify](http://www.theadvocate.com/louisiana_flood_2016/article_a7689806-6946-11e6-a681-ab59c458f55c.html?sr_source=lift_amplify)>
- 964 American Red Cross: Louisiana Flooding: Red Cross Shelters 10,000+ After Worst Disaster Since Superstorm
965 Sandy. *American Red Cross*, viewed August 23 2016, [http://www.redcross.org/news/press-release/Louisiana-
966 Flooding-Red-Cross-Shelters-10000-After-Worst-Disaster-Since-Superstorm-Sandy](http://www.redcross.org/news/press-release/Louisiana-Flooding-Red-Cross-Shelters-10000-After-Worst-Disaster-Since-Superstorm-Sandy)
- 967 American Red Cross: Needs of People in Louisiana Remain Great; Red Cross Still Sheltering 7,000+, Serving
968 Thousands of Meals. *American Red Cross*, viewed 23 August 2016, <[http://www.redcross.org/news/press-
969 release/Needs-of-People-in-Louisiana-Remain-Great-Red-Cross-Still-Sheltering-7000-Serving-Thousands-of-
970 Meals](http://www.redcross.org/news/press-release/Needs-of-People-in-Louisiana-Remain-Great-Red-Cross-Still-Sheltering-7000-Serving-Thousands-of-Meals)>.
- 971 Broach, D.: How many houses, people flooded in Louisiana? *NOLA*, viewed 24 August 2016,
972 <http://www.nola.com/weather/index.ssf/2016/08/how_many_people_houses_were_fl.html>.
- 973 Bromwich, J.E.: Flooding in the South Looks a Lot Like Climate Change, *The New York Times*, viewed 24
974 August 2016, <<http://www.nytimes.com/2016/08/17/us/climate-change-louisiana.html>>.
- 975 Burton, J. and A. Demas: Six streamgages Set peaks of record and 50 stations were overtopped by floodwaters.
976 *USGS*, viewed 22 August 2016, <<https://www.usgs.gov/news/usgs-records-historic-flooding-south-louisiana>>.
- 977 Centre for Research on the Epidemiology of Disasters (CRED): The Human Cost of Natural Disasters 2015, A
978 Global Perspective; ReliefWeb, viewed on 29 August 2016
979 http://reliefweb.int/sites/reliefweb.int/files/resources/PAND_report.pdf
- 980 Chen, C.-T., and Knutson, T.: On the verification and comparison of extreme rainfall indices from climate
981 models. *J. Climate*, 21 (7), 1605–1621, 2008.
- 982 Christidis, N., Stott, P.A., Scaife, A.A., Arribas, A., Jones, G.S., Copesey, D., Knight, J.R. and Tennant, W.J.: A
983 new HadGEM3-A-based system for attribution of weather-and climate-related extreme events. *J. Climate*,
984 26(9), pp.2756-2783, 2013.
- 985 Collins, M., Knutti, R., Arblaster, J., Dufresne, J.-L., Fichefet, T., Friedlingstein, P., Gao, X., Gutowski, W.J.,
986 Johns, T., Krinner, G., Shongwe, M., Tebaldi, C., Weaver, A.J., and Wehner, M.: Long-term Climate Change:
987 Projections, Commitments and Irreversibility. In *Climate Change 2013: The Physical Science Basis, Contribution of Working Group I to the Fifth Assessment Report of the Intergovernmental Panel on Climate Change*. [Stocker, T.F., Qin, D., Plattner, G.-K., Tignor, M., Allen, S.K., Boschung, J., Nauels, A., Xia, Y., Bex, V., and Midgley, P.M. (eds.)]. Cambridge University Press, Cambridge, United Kingdom and New York, NY, USA. 2013.
- 992 Coles, S.: *An Introduction to Statistical Modeling of Extreme Values*, Springer Series in Statistics, London, UK,
993 2001.
- 994 Cutlip, K 2013, 'Weather Front', *Weatherwise*, 66, 2, p. 6, MAS Ultra - School Edition, EBSCOhost, viewed 29
995 August 2016.
- 996 Dai, A.: Precipitation characteristics in eighteen coupled climate models. *J. Climate*, 19(18), 4605-4630, 2006.
- 997 Davies, R.: Louisiana Rivers at Record Levels, President Declares Major Disaster. *Floodlist*, viewed 23 August
998 2016, <<http://floodlist.com/america/usa/usa-louisiana-rivers-record-levels-president-declares-major-disaster>>.
- 999 Delworth, T.L., Broccoli, A.J., Rosati, A., Stouffer, R.J., Balaji, V., Beesley, J.A., Cooke, W.F., Dixon, K.W.,
1000 Dunne, J., Dunne, K.A. and Durachta, J.W., Findell, K., Ginoux, P., Gnanadesikan, A., Gordon, C.T., Griffies, S.,
1001 Gudgel, R., Harrison, M., Held, I., Hemler, R., Horowitz, L., Klein, S., Knutson, T., Kushner, P.,
1002 Langenhorst, A., Lee, H.-C., Lin, S.-J., Lu, J., Malyshev, S., Milly, P.C.D., Ramaswamy, V., Russell, J.,
1003 Schwarzkopf, M.D., Shevliakova, E., Sirutis, j., Spelman, M., Stern, W., Winton, M., Wittenberg, A., Wyman,

1004 B., Zeng, F., Zhang, R.: GFDL's CM2 global coupled climate models. Part I: Formulation and simulation
1005 characteristics. *J. Climate*, 19(5), 643-674, 2006.

1006 Delworth, T.L., Rosati, A., Anderson, W., Adcroft, A.J., Balaji, V., Benson, R., Dixon, K., Griffies, S.M., Lee,
1007 H.C., Pacanowski, R.C., Vecchi, G.A., Wittenberg, A.T., Zeng, F., and Zhang, R.: Simulated climate and
1008 climate change in the GFDL CM2. 5 high-resolution coupled climate model. *J. Climate*, 25(8), 2755-2781,
1009 2012.

1010 Delworth, T.L., Zeng, F., Rosati, A., Vecchi, G.A. and Wittenberg, A.T.: A link between the hiatus in global
1011 warming and North American drought. *J. Climate*, 28(9), 3834-3845, 2015.

1012 [Efron, B. and Tibshirani, R. J., 1998. *An introduction to the bootstrap*, Chapman and Hall, New York. 439pp.](#)

1013 Eggert, B., Berg, P., Haerter, J.O., Jacob, D. and Moseley, C.: Temporal and spatial scaling impacts on extreme
1014 precipitation. *Atmospheric Chemistry and Physics*, 15(10), 5957-5971, 2015.

1015 Emanuel, K., and Sobel, A.: Response of tropical sea surface temperature, precipitation, and tropical cyclone-
1016 related variables to changes in global and local forcing. *J. of Advances in Modeling Earth Systems*,
1017 doi:10.1002/jame.20032, 2013.

1018 Emanuel, K., Solomon, S., Folini, D., Davis, S., and Cagnano, C.: Influence of Tropical Tropopause Layer
1019 Cooling on Atlantic Hurricane Activity. *J. Climate*, doi:10.1175/JCLI-D-12-00242.1, 2013

1020 FEMA: Federal Support for Louisiana Continues, \$127 Million in Financial Assistance Provided to Louisiana
1021 Flood Survivors So Far. FEMA, viewed 23 August 2016, <[https://www.fema.gov/news-
1022 release/2016/08/23/federal-support-louisiana-continues-127-million-financial-assistance](https://www.fema.gov/news-release/2016/08/23/federal-support-louisiana-continues-127-million-financial-assistance)>

1023 Flato, G., Marotzke, J., Abiodun, B., Braconnot, P., Chou, S.C., Collins, W.J., Cox, P., Driouech, F.,
1024 Emori, S., Eyring, V. and Forest, C., Gleckler, P., Guilyardi, E., Jakob, C., Kattsov, V., Reason, C.,
1025 Rummukainen, M.: *Evaluation of Climate Models. In: Climate Change 2013: The Physical Science Basis.*
1026 *Contribution of Working Group I to the Fifth Assessment Report of the Intergovernmental Panel on*
1027 *Climate Change*. Climate Change 2013, 5,741-866, 2013.

1028 Forster, P. M., T. Andrews, P. Good, J. M. Gregory, L. S. Jackson, and M. Zelinka: Evaluating adjusted
1029 forcing and model spread for historical and future scenarios in the CMIP5 generation of climate models, *J.*
1030 *Geophys. Res. Atmos.*, 118, 1139–1150, doi:10.1002/jgrd.50174, 2013.

1031 Gandin, L. S., and R. Hardin: *Objective analysis of meteorological fields*, Vol. 242. Israel program for scientific
1032 translations Jerusalem, 1965.

1033 GISTEMP Team: GISS Surface Temperature Analysis (GISTEMP). NASA Goddard Institute for Space Studies.
1034 Dataset accessed 2016-08-08 at <<http://data.giss.nasa.gov/gistemp/>>.

1035 Haarsma, R. J., Roberts, M., Vidale, P. L., Senior, C. A., Bellucci, A., Bao, Q., Chang, P., Corti, S.,
1036 Fučkar, N. S., Guemas, V., von Hardenberg, J., Hazeleger, W., Kodama, C., Koenigk, T., Leung, L. R.,
1037 Lu, J., Luo, J.-J., Mao, J., Mizielinski, M. S., Mizuta, R., Nobre, P., Satoh, M., Scoccimarro, E., Semmler,
1038 T., Small, J., and von Storch, J.-S.: High Resolution Model Intercomparison Project (HighResMIP),
1039 *Geosci. Model Dev. Discuss.*, doi:10.5194/gmd-2016-66, in review, 2016.

1040 Hansen, J., Ruedy, R., Sato, M. and Lo, K.: Global surface temperature change. *Reviews of Geophysics*, 48(4),
1041 2010.

1042 Harris, L.M, Lin, S.-J., and Tu, C.Y.: High resolution climate simulations using GFDL HiRAM with a stretched
1043 global grid. *J. Climate*, 29, 4293–4314, 2016.

1044 Hawkins, E. and Sutton, R.: The potential to narrow uncertainty in regional climate predictions. *Bulletin of the*
1045 *American Meteorological Society*, 90(8), 1095, 2009.

1046 Hazeleger, W. Wang, X., Severijns, C., Stefanescu, S., Bintanja, R., Sterl, A., Wyser, K., Semmler, T, Yang, S.,
1047 Van den Hurk, B., Van Noije, T., Van der Linden, E., Van der Wiel, K.: EC-Earth V2.2: description and
1048 validation of a new seamless earth system prediction model. *Clim.Dyn.*, 39, 2611-2629, 2012.

1049 Hazeleger, W., Wouters, B., Oldenborgh, G.J., Corti, S., Palmer, T., Smith, D., Dunstone, N., Kröger, J.,
1050 Pohlmann, H. and Storch, J.S.: Predicting multiyear north atlantic ocean variability. *Journal of Geophysical*
1051 *Research: Oceans*, 118(3), 1087-1098, 2013.

1052 Herscher, R.: “Flooding in Louisiana Raises Questions About Timing, Urgency of Warnings” *NPR*, viewed 29
1053 August 2016, <[http://www.npr.org/sections/thetwo-way/2016/08/22/490916070/flooding-in-louisiana-raises-](http://www.npr.org/sections/thetwo-way/2016/08/22/490916070/flooding-in-louisiana-raises-questions-about-timing-urgency-of-warnings)
1054 [questions-about-timing-urgency-of-warnings](http://www.npr.org/sections/thetwo-way/2016/08/22/490916070/flooding-in-louisiana-raises-questions-about-timing-urgency-of-warnings)>.

1055 Higgins, R. W., W. Shi, E. Yarosh, and R. Joyce: Improved United States precipitation quality control system
1056 and analysis. NOAA, National Weather Service, National Centers for Environmental Prediction, *Climate*
1057 *Prediction Center Atlas*, 2000.

1058 Huang, B., Banzon, V.F., Freeman, E., Lawrimore, J., Liu, W., Peterson, T.C., Smith, T.M., Thorne, P.W.,
1059 Woodruff, S.D. and Zhang, H.M.: Extended reconstructed sea surface temperature version 4 (ERSST. v4). Part
1060 I: upgrades and intercomparisons. *J. Climate*, 28(3), 911-930, 2015.

1061 Jia, L., Yang, X., Vecchi, G.A., Gudgel, R.G., Delworth, T.L., Rosati, A., Stern, W.F., Wittenberg, A.T.,
1062 Krishnamurthy, L., Zhang, S. and Msadek, R.: Improved seasonal prediction of temperature and precipitation
1063 over land in a high-resolution GFDL climate model. *J. Climate*, 28(5), 2044-2062, 2015.

1064 Jia, L., Vecchi, G.A., Yang, X., Gudgel, R., Delworth, T., Stern, W., Paffendorf, K., Underwood, S., Zeng, F.:
1065 The Roles of Radiative Forcing, Sea Surface Temperatures, and Atmospheric and Land Initial Conditions in
1066 U.S. Summer Warming Episodes. *J. Climate*, doi:10.1175/JCLI-D-15-0471.1, 2016.

1067 Kalnay, E., Kanamitsu, M., Kistler, R., Collins, W., Deaven, D., Gandin, L., Iredell, M., Saha, S., White, G.,
1068 Woollen, J. and Zhu, Y.: The NCEP/NCAR 40-year reanalysis project. *Bulletin of the American meteorological*
1069 *Society*, 77(3), 437-471, 1996.

1070 Katsman, C.A., Hazeleger, W., Drijfhout, S.S., van Oldenborgh, G.J. and Burgers, G.: Climate scenarios of sea
1071 level rise for the northeast Atlantic Ocean: a study including the effects of ocean dynamics and gravity changes
1072 induced by ice melt. *Climatic Change*, 91(3-4), 351-374, 2008.

1073 Keim, B.D. and Faiers, G.E.: Heavy rainfall distributions by season in Louisiana: Synoptic interpretations and
1074 quantile estimates. *Water Resources Bulletin*, 32(1), 117-124, 1996.

1075 Kirtman, B., Power, S.B., Adedoyin, J.A., Boer, G.J., Bojariu, R., Camilloni, I., Doblas-Reyes, F.J., Fiore,
1076 A.M., Kimoto, M., Meehl, G.A., Prather, M., Sarr, A., Schär, C., Sutton, R., Van Oldenborgh, G.J., Vecchi, G.,
1077 and Wang, H.-J.: Near-term climate change: projections and predictability. In *Climate Change 2013: The*
1078 *Physical Science Basis, Contribution of Working Group I to the Fifth Assessment Report of the*
1079 *Intergovernmental Panel on Climate Change*. [Stocker, T.F., Qin, D., Plattner, G.-K., Tignor, M., Allen, S.K.,
1080 Boschung, J., Nauels, A., Xia, Y., Bex, V., and Midgley, P.M. (eds.)]. Cambridge University Press, Cambridge,
1081 United Kingdom and New York, NY, USA. 2013.

1082 Knapp, K.R., Kruk, M.C., Levinson, D.H., Diamond, H.J. and Neumann, C.J.: The international best track
1083 archive for climate stewardship (IBTrACS). *Bulletin of the American Meteorological Society*, 91(3), 363, 2010.

1084 Knutson, T.R., Sirutis, J.J., Vecchi, G.A., Garner, S., Zhao, M., Kim, H.S., Bender, M., Tuleya, R.E., Held, I.M.
1085 and Villarini, G.: Dynamical downscaling projections of twenty-first-century Atlantic hurricane activity: CMIP3
1086 and CMIP5 model-based scenarios. *J. Climate*, 26(17), 6591-6617, 2013.

1087 Krishnamurthy, L., Vecchi, G., Msadek, R., Wittenberg, A., Delworth, T., and Zeng, F.: The Seasonality of the
1088 Great Plains Low-Level Jet and ENSO Relationship. *J. Climate*. doi:10.1175/JCLI-D-14-00590.1, 2015.

1089 Lehmann, J., Coumou, D. and Frieler, K.: Increased record breaking precipitation events under global
1090 warming. *Climatic Change*, 132(4), 501-505, doi:10.1007/s10584-015-1434-y, 2015.

1091 Lenderink, G. and Attema, J.: A simple scaling approach to produce climate scenarios of local precipitation
1092 extremes for the Netherlands. *Environmental Research Letters*, 10(8), 085001, 2015.

1093 Little, C.M., Horton, R.M., Kopp, R.E., Oppenheimer, M., Vecchi, G.A., and Villarini, G.: Joint projections of
1094 US East Coast sea level and storm surge. *Nature Climate Change*. doi:10.1038/nclimate2801, 2015.

1095 Lin, N., Emanuel, K., Oppenheimer, M. and Vanmarcke, E.: Physically based assessment of hurricane surge
1096 threat under climate change. *Nature Climate Change*, 2(6), 462-467, 2012.

1097 Lin, N., Lane, P., Emanuel, K.A., Sullivan, R.M., and Donnelly, J.P.: Heightened hurricane surge risk in
1098 northwest Florida revealed from climatological-hydrodynamic modeling and paleorecord reconstruction. *J.*
1099 *Geophys. Res. (Atmospheres)*, doi:10.1002/2014JD021584, 2014

1100 Massey, N., Jones, R., Otto, F.E.L., Aina, T., Wilson, S., Murphy, J.M., Hassell, D., Yamazaki, Y.H., and M.R.
1101 Allen: weather@home - development and validation of a very large ensemble modelling system for probabilistic
1102 event attribution. *Q. J. Royal Met. Soc.*, doi:10.1002/qj.2455, 2015.

1103 Menne, M.J., I. Durre, R.S. Vose, B.E. Gleason, and T.G. Houston: An overview of the Global Historical
1104 Climatology Network-Daily Database. *Journal of Atmospheric and Oceanic Technology*, 29, 897-910, 2012.
1105

1106 Menne, M.J., I. Durre, B. Korzeniewski, S. McNeal, K. Thomas, X. Yin, S. Anthony, R. Ray, R.S. Vose,
1107 B.E.Gleason, and T.G. Houston: Global Historical Climatology Network-Daily (GHCN-Daily), Version 3.22.
1108 NOAA National Climatic Data Center. <http://doi.org/10.7289/V5D21VHZ> 19 August 2016.

1109 De Michele, C. and Salvadori, G.: On the derived flood frequency distribution: analytical formulation and the
1110 influence of antecedent soil moisture condition. *Journal of Hydrology*, 262(1), 245-258, 2002.

1111 Milman, O.: Disasters like Louisiana floods will worsen as planet warms, scientists warn, *The Guardian*, viewed
1112 24 August 2016, <<https://www.theguardian.com/environment/2016/aug/16/louisiana-flooding-natural-disaster-weather-climate-change>>.
1113

1114 Moftakhari, H.R., AghaKouchak, A., Sanders, B.F., Feldman, D.L., Sweet, W., Matthew, R.A. and Luke, A.:
1115 Increased nuisance flooding along the coasts of the United States due to sea level rise: Past and future. *Geophys.*
1116 *Res. Lett.*, 42(22), 2015.

1117 Msadek, R., Vecchi, G.A., Winton, M., Gudgel, R.: Importance of initial conditions in seasonal predictions of
1118 Arctic sea ice extent. *Geophys. Res. Lett.*, DOI: 10.1002/2014GL060799, 2014.

1119 Murakami, H., and Wang, B.: Future Change of North Atlantic Tropical Cyclone Tracks: Projection by a 20-
1120 km-Mesh Global Atmospheric Model. *J. Climate*, doi:10.1175/2010JCLI3338.1, 2010.

1121 Murakami, H., Vecchi, G.A., Underwood, S., Delworth, T., Wittenberg, A.T., Anderson, W., Chen, J.-H.,
1122 Gudgel, R., Harris, L., Lin, S.-J., and Zeng, F.: Simulation and prediction of Category 4 and 5 hurricanes in the
1123 high-resolution GFDL HiFLOR coupled climate model. *J. Climate*, doi:10.1175/JCLI-D-15-0216.1, 2015.

1124 Murakami, H., Vecchi, G.A., Villarini, G., ., Delworth, T., Gudgel, R., Underwood, S.D., Yang, X., Zhang, W.,
1125 Lin, S.-J.: Seasonal Forecasts of Major Hurricanes and Landfalling Tropical Cyclones using a High-Resolution
1126 GFDL Coupled Climate Model. *J. Climate*, 10.1175/JCLI-D-16-0233.1, 2016.

1127 National Weather Service: Southern and Eastern U.S. Heavy Rainfall, storm summaries 1-19, viewed 23 August
1128 2016, <http://www.wpc.ncep.noaa.gov/winter_storm_summaries/storm15/storm15_archive.shtml> and New
1129 Orleans area forecast discussions (PIL=AFDLIX), viewed 24 August 2016,
1130 <<https://mesonet.agron.iastate.edu/wx/afos/>>.

1131 O’Gorman, P.A.: Precipitation extremes under climate change. *Current climate change reports*, 1(2), 49-59,
1132 2015.

1133 Otto, F.E., Van Oldenborgh, G.J., Eden, J., Stott, P.A., Karoly, D.J. and Allen, M.R.: The attribution question.
1134 *Nature Climate Change*, 6(9), pp.813-816, 2016.

1135 Pascale, S., Bordoni, S., Kapnick, S.B., Vecchi, G.A., Jia, L., Delworth, T.L., Underwood, S. Anderson, W.:
1136 The impact of horizontal resolution on North American monsoon Gulf of California moisture surges in a suite
1137 of coupled global climate models. *J. Climate*, doi:10.1175/JCLI-D-16-0199.1, 2016.

1138 Pinter, N., van der Ploeg, R.R., Schweigert, P. and Hoefler, G.: Flood magnification on the River Rhine.
1139 *Hydrological Processes*, 20(1), 147-164, 2006.

1140 Putman, W. M., and S.-J. Lin: Finite-volume transport on various cubed-sphere grids. *Journal of Computational*
1141 *Physics*, 227 (1), 55–78, 2007.

1142 Rantz, S.E.: Measurement and computation of streamflow: volume 2, computation of discharge (No. 2175).
1143 USGPO, 1982. Available at: <http://pubs.usgs.gov/wsp/wsp2175/pdf/WSP2175_voll1a.pdf>.

1144 Rayner, N.A., Parker, D.E., Horton, E.B., Folland, C.K., Alexander, L.V., Rowell, D.P., Kent, E.C. and Kaplan,
1145 A.: Global analyses of sea surface temperature, sea ice, and night marine air temperature since the late
1146 nineteenth century. *Journal of Geophysical Research: Atmospheres*, 108(D14), doi:10.1029/2002JD002670,
1147 2003.

1148 Stafford, Robert, T., Stafford disaster relief and emergency assistance act. *Public Law*, 10(30), 106-390, 2000.

1149 Scherrer, S.C., Fischer, E.M., Posselt, R., Liniger, M.A., Croci- Maspoli, M. and Knutti, R.: Emerging trends in
1150 heavy precipitation and hot temperature extremes in Switzerland. *Journal of Geophysical Research:*
1151 *Atmospheres*, doi:10.1002/2015JD024634, 2016.

1152 Schleifstein, M.: Louisiana Flood of 2016 resulted from '1,000-year' rain in 2 days, *NOLA*, viewed at 23 August
1153 2016, <http://www.nola.com/weather/index.ssf/2016/08/louisiana_flood_of_2016_result.html>.

1154 Sterl, A., Brink, H.V.D., Vries, H.D., Haarsma, R. and Meijgaard, E.V.: An ensemble study of extreme storm
1155 surge related water levels in the North Sea in a changing climate. *Ocean Science*, 5(3), 369-378, 2009.

1156 Strum, B.: Damage Grows from Louisiana Flood. *Wall Street Journal*, viewed at 23 August 2016,
1157 <<http://www.wsj.com/articles/damage-grows-from-louisiana-flood-1471803140>>.

1158 Taylor, K.E., Stouffer, R.J. and Meehl, G.A.: An overview of CMIP5 and the experiment design. *Bulletin of the*
1159 *American Meteorological Society*, 93(4), 485-498, 2012.

1160 Trambly, Y., Bouvier, C., Martin, C., Didon-Lescot, J.F., Todorovik, D. and Domergue, J.M.: Assessment of
1161 initial soil moisture conditions for event-based rainfall-runoff modelling. *Journal of Hydrology*, 387(3), 176-
1162 187, 2010.

1163 Van der Wiel, K., Kapnick S.B., Vecchi G.A., Cooke, W.F., Delworth T.L., Jia L., Murakami H., Underwood
1164 S., and Zeng F.: The resolution dependence of contiguous US precipitation extremes in response to CO2
1165 forcing. *J. Climate*, doi: 10.1175/JCLI-D-16-0307.1, 2016.

1166 Van Oldenborgh, G. J., Otto, F. E. L., Haustein, K., and Cullen, H.: Climate change increases the probability of
1167 heavy rains like those of storm Desmond in the UK – an event attribution study in near-real time, *Hydrol. Earth*
1168 *Syst. Sci. Discuss.*, 12, 13197-13216, doi:10.5194/hessd-12-13197-2015, in review, 2015.

1169 Van Oldenborgh, G. J., Philip, S., Aalbers, E., Vautard, R., Otto, F., Haustein, K., Habets, F., Singh, R., and
1170 Cullen, H.: Rapid attribution of the May/June 2016 flood-inducing precipitation in France and Germany to
1171 climate change, *Hydrol. Earth Syst. Sci. Discuss.*, doi:10.5194/hess-2016-308, in review, 2016.

1172 Van Vuuren, D.P., Edmonds, J., Kainuma, M., Riahi, K., Thomson, A., Hibbard, K., Hurtt, G.C., Kram, T.,
1173 Krey, V., Lamarque, J.F., Masui, T., Meinshausen, M., Nakicenovic, N., Smith, S., and Rose, S.: The
1174 representative concentration pathways: an overview. *Climatic change*, 109, 5-31, 2011.

1175 Vecchi, G.A., Fueglistaler, S., Held, I.M., Knutson, T.R., and Zhao, M.: Impacts of Atmospheric Temperature
1176 Changes on Tropical Cyclone Activity. *J. Climate* doi: 10.1175/JCLI-D-12-00503.1, 2013.

1177 Vecchi, G.A., and Soden. B.J.: Effect of remote sea surface temperature change on tropical cyclone potential
1178 intensity, *Nature*, 450, 1066-1070 doi:10.1038/nature06423, 2007.

1179 Vecchi, G.A., Delworth, T., Gudgel, R., Kapnick, S.B., Rosati, A., Wittenberg, A.T., Zeng, F., Anderson, W.,
1180 Balaji, V., Dixon, K. Jia, L., Kim, H-S, Krishnamurthy, L., Msadek, R., Stern, W.F, Underwood, S.D., Villarini,
1181 G., Yang, X., and Zhang, S.: On the seasonal forecasting of regional tropical cyclone activity. *J. Climate*,
1182 27(21), 7994-8016, 2014.

1183 Villarini, G., Goska, R., Smith, J.A. and Vecchi, G.A.: North Atlantic tropical cyclones and US flooding.
1184 *Bulletin of the American Meteorological Society*, 95(9), 1381-1388, 2014.

1185 Walsh, K., Camargo, S., Vecchi, G., Daloz, A., Elsner, J., Emanuel, K., Horn, M., Lim, Y.-K., Roberts, M.,
1186 Patricola, C., Scoccimarro, E., Sobel, A., Strazzo, S., Villarini, G., Wehner, M., Zhao, M., Kossin, J., LaRow,
1187 T., Oouchi, K., Schubert, S., Wang, H., Bacmeister, J., Chang, P., Chauvin, F., Jablonowski, C., Kumar, A.,
1188 Murakami, H., Ose, T., Reed, K., Saravanan, R., Yamada, Y., Zarzycki, C., Vidale, P., Jonas, J., Henderson, N.:
1189 Hurricanes and climate: the U.S. CLIVAR working group on hurricanes. *Bull. Amer. Meteorol. Soc.*
1190 doi:10.1175/BAMS-D-13-00242.1, 2015.

1191 Yang, X., Vecchi, G.A., Gudgel, R.G., Delworth, T.L., Zhang, S., Rosati, A., Jia, L., Stern, W.F., Wittenberg,
1192 A.T., Kapnick, S. and Msadek, R.: Seasonal predictability of extratropical storm tracks in GFDL's high-
1193 resolution climate prediction model. *J. Climate*, 28(9), 3592-3611, 2015.

1194 Zhang, W., Vecchi, G.A., Murakami, H., Delworth, T., Wittenberg, A.T., Anderson, W., Rosati, A.,
1195 Underwood, S., Harris, L., Gudgel, R., Lin, S.-J., Villarini, G., and Chen, J.-H.: Improved Simulation of
1196 Tropical Cyclone Responses to ENSO in the Western North Pacific in the High-Resolution GFDL HiFLOR
1197 Coupled Climate Model. *J. Climate*, doi:10.1175/JCLI-D-15-0475.1, 2016.

1198 Zhang, W., Leung, Y. and Fraedrich, K.: Different El Niño types and intense typhoons in the Western North
1199 Pacific. *Climate Dynamics*, 44(11-12), 2965-2977, 2015.